

AD-A179 477

INVESTIGATION OF SHROUDED NOZZLE EXIT PRESSURE CHANGES  
(U) AIR FORCE INST OF TECH WRIGHT-PATTERSON AFB OH  
SCHOOL OF ENGINEERING D C RODGERS DEC 86

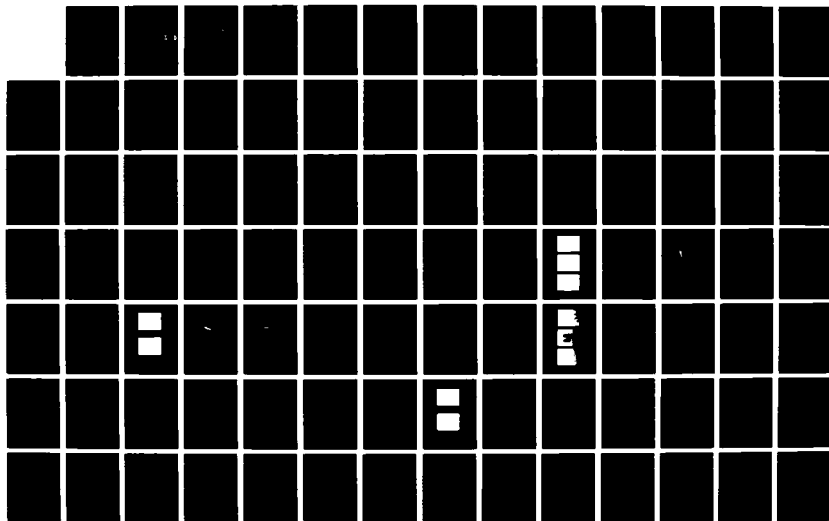
1/2

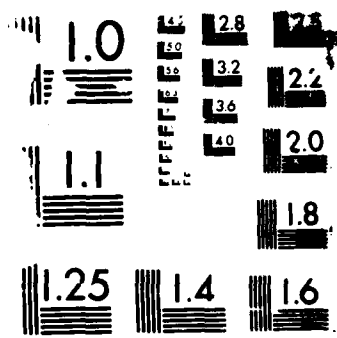
UNCLASSIFIED

AFIT/GAE/RA/86D-15

F/B 28/4

ML





M1

DTIC FILE COPY

1

AD-A179 477



DTIC  
 ELECTE  
 APR 17 1987  
 S D

INVESTIGATION OF SHROUDED NOZZLE  
 EXIT PRESSURE CHANGES  
 THESIS  
 Douglas C. Rodgers  
 Captain, USAF  
 AFIT/GAE/AA/86D-15

**DISTRIBUTION STATEMENT A**  
 Approved for public release;  
 Distribution Unlimited

DEPARTMENT OF THE AIR FORCE  
 AIR UNIVERSITY  
**AIR FORCE INSTITUTE OF TECHNOLOGY**

Wright-Patterson Air Force Base, Ohio

87 4 16 046

1

AFIT/GAE/AA/86

DTIC  
ELECTED  
APR 17 1987  
S D

INVESTIGATION OF SHROUDED NOZZLE

EXIT PRESSURE CHANGES

THESIS

Douglas C. Rodgers  
Captain, USAF

AFIT/GAE/AA/86D-154

Approved for public release; distribution unlimited

AFIT/GAE/AA/86D-15

INVESTIGATION OF SHROUDED NOZZLE EXIT PRESSURE CHANGES

THESIS

Presented to the Faculty of the School of Engineering  
of the Air Force Institute of Technology  
Air University  
In Partial Fulfillment of the  
Requirements for the Degree of  
Master of Science in Aeronautical Engineering



Douglas C. Rodgers, B.S.  
Captain, USAF

December 1986

Accession For	
NTIS CRA&I	<input checked="" type="checkbox"/>
DTIC TAB	<input type="checkbox"/>
Unannounced	<input type="checkbox"/>
Justification	
By	
Distribution/	
Availability Codes	
Dist	Avail and/or Special
A-1	

Approved for public release; distribution unlimited

## Preface

I selected an experimental thesis in order to practically apply the knowledge that I have acquired over the last year and a half. This study on clustered, shrouded rocket nozzles more than adequately met this goal.

Completing this project would have been impossible without the help of my thesis advisor, Dr. W. C. Elrod. Not only did he provide guidance on the theoretical aspects of the thesis but his practical knowledge of experimental techniques and problem solving abilities were significant in the accomplishment of my goal. As I had never done experimental work prior to this thesis, I can state that completing this investigation would have been impossible without Dr. Elrod's gracious assistance. Lt Col Jumper provided strong support in developing my understanding of the supporting theory and Capt Carlson provided strong moral encouragement when the project seemed most overwhelming.

I would like to thank the aeronautical and astronautical laboratory technicians for their support throughout my labors. Messrs. Nick Yardich, Jay Anderson, and Leroy Cannon were invaluable in providing logistic support, setting up the required hardware, and solving technical equipment and instrumentation problems. Messrs. John Brohas, Tim Hancock, and Ron Ruley of the AFIT Fabrication shop were also outstanding contributors to my thesis. Their work on the

instrumentation collar and the nozzle blocks was superb, a true tribute to these master craftsmen.

Finally, this thesis would have never been completed without the sacrifices and loving support of my wife, Maralee, and children, Christopher, Timothy, and Kristen, during these last eighteen months. They gave me the strength to finish a difficult task.

Douglas C. Rodgers

Computer: Commodore 64  
Software: Easy Script  
Printer: Star PowerType

## Table of Contents

	Page
Preface .....	ii
List of Figures .....	v
List of Tables .....	viii
Abstract .....	ix
I. Introduction .....	1
Theory .....	2
Objectives .....	5
II. Experimental Apparatus .....	8
Flow System .....	10
Instrumentation Collar .....	10
Test Section .....	11
Nozzle Blocks .....	13
Configurations .....	13
Instrumentation .....	18
Schlieren System .....	20
III. Data Acquisition and Reduction System .....	22
IV. Experimental Procedure .....	30
Calibration .....	30
Test Procedure .....	31
V. Results and Discussion .....	34
Base Pressures .....	37
Shroud Pressures .....	51
VI. Conclusions .....	59
VII. Recommendations .....	61
Bibliography .....	62
Appendix A .....	63
Appendix B .....	75
Vita .....	90

## List of Figures

Figure	Page
1. Nozzle Operating Diagram (3:8) .....	6
2. System Schematic .....	9
3. Test Section .....	12
4. Nozzle Block 1 (AR=8:1) .....	14
5. Nozzle Block 2 (AR=8:1) .....	15
6. Nozzle Block 3 (AR=4:1) .....	16
7. Nozzle Block 4 (AR=3:1) .....	17
8. Schlieren System (8:13) .....	21
9. Hardware Schematic (8:16) .....	24
10. Simplified HP6901S System (8:17) .....	25
11. Data Flow Path (8:19) .....	27
12. Operational Flow of HP6901S Menu Utilities .....	28
13. Instrumentation Amplifier .....	32
14. Base Plate and Channel Flow (8:29) .....	35
15. Schlieren Series for Configuration 1A .....	38
16. P3 vs PR (Con1A) .....	39
17. P4 vs PR (Con1A) .....	40
18. P5 vs PR (Con1A) .....	41
19. P3 vs PR (Con1B) .....	43
20. Schlieren Series for Nozzle Block 2 .....	45
21. P3 vs PR (Con3A) .....	46
22. P3 vs PR (Con3B) .....	47
23. P4 vs PR (Con4A) .....	49
24. P4 vs PR (Con4B) .....	50

25.	Schlieren Series for Nozzle Block 4 .....	52
26.	P9 vs PR (Con1A) .....	53
27.	P9 vs PR (Con1B) .....	55
28.	P5 vs PR (Con3A) .....	56
29.	P5 vs PR (Con3B) .....	57
A-1.	Schlieren Series for Configuration 1B .....	64
A-2.	PR vs Time (Con2A) .....	65
A-3.	P3 vs PR (Con2A) .....	66
A-4.	P4 vs PR (Con2A) .....	67
A-5.	P5 vs PR (Con2A) .....	68
A-6.	P6 vs PR (Con2A) .....	69
A-7.	PR vs Time (Con2B) .....	70
A-8.	P3 vs PR (Con2B) .....	71
A-9.	P4 vs PR (Con2B) .....	72
A-10.	P5 vs PR (Con2B) .....	73
A-11.	P6 vs PR (Con2B) .....	74
B-1.	PR vs Time (Con2A) .....	76
B-2.	P7 vs PR (Con2A) .....	77
B-3.	P8 vs PR (Con2A) .....	78
B-4.	P9 vs PR (Con2A) .....	79
B-5.	PR vs Time (Con2B) .....	80
B-6.	P7 vs PR (Con2B) .....	81
B-7.	P8 vs PR (Con2B) .....	82
B-8.	P9 vs PR (Con2B) .....	83
B-9.	P6 vs PR (Con4B) .....	84
B-10.	P7 vs PR (Con4B) .....	85

B-11. P8 vs PR (Con4B) .....86  
B-12. P9 vs PR (Con4B) ..... 87  
B-13. P10 vs PR (Con4B) ..... 88  
B-14. P11 vs PR (Con4B) ..... 89

List of Tables

Table	Page
I. Configurations .....	19
II. Test Instrumentation .....	23

ABSTRACT

This research involved the investigation of shrouded two- and three-dimensional, supersonic, cold flow nozzles. Altitudes up to 87,000 feet were simulated and nozzle inlet to ambient pressure ratios up to 400 were used. Pressure measurements were made along the nozzle exit plane and the shroud walls to determine the effect shrouding has on exit base pressure and the pressure distribution along the shroud walls. Comparisons were made in the blowdown wind tunnel using a variety of nozzle types, nozzle area ratios, and shroud lengths. Schlieren photography techniques were used to provide additional information for interpretation of the wind tunnel data.

The results of this study are that the pressure fields in the base region of the nozzle and along the shroud walls are dependent upon the geometry of the configuration and the operating altitude. The shroud wall pressures were found to act in the same manner as the base pressures by first maintaining a fairly constant pressure value until the chamber to ambient pressure ratio reached some critical value. When this condition occurred, the flow separated from the shroud with a resulting increase in the shroud wall pressures. Potential increases in nozzle assembly

performance are possible from changing effective nozzle exit area and the resulting changes in the flow gas dynamics.

X

INVESTIGATION OF SHROUDED NOZZLE  
EXIT PRESSURE CHANGES

I INTRODUCTION

Clustered rocket nozzle research has been going on since the late 1950's. Works by Goethert (4) and Holmes and Matz (6) indicate that shrouded, clustered nozzles may have improved performance over unshrouded nozzles. AFIT studies by Moran (8) and Bjurstrom (2) examined the effects of shrouds and exhaust plume interaction on rocket nozzle performance. Bjurstrom's work, the earlier of the two AFIT studies, investigated jet exhaust interactions and their affect upon the nozzle base pressures with two-dimensional clustered rocket nozzles. He found clustered nozzles have a high pressure region trapped between the interacting exhaust plumes, possibly providing an additional pressure term acting over the nozzle base area. Moran continued this line of study and expanded it to include shrouded and clustered, three-dimensional nozzles. Shrouds were found to influence the nozzle inlet to ambient back pressure ratio for flow separation from the shroud walls and to affect the nozzle exit plane base pressures. A difference was noted between the base pressures of shrouded and unshrouded models with the

shrouded base pressures remaining nearly constant until the separation pressure ratio was reached while the unshrouded base pressures gradually increased as the nozzle inlet to ambient back pressure ratio dropped. This current investigation will go one step further and evaluate the influence of various shroud lengths and nozzle combinations on not only the base pressures but also the shroud wall pressure distributions.

Because of the potential performance increase, new missile designs may include shrouded, clustered nozzles. Additional research is necessary to determine the effects of the shrouded, clustered nozzle exhaust flow field so that it will be possible to predict and use any performance improvement. Evaluation of the shroud wall pressure distribution can provide valuable information to be used in the determination of the usefulness of shrouding clustered rocket nozzle assemblies.

### Theory

Using the momentum equation, a relation for nozzle thrust can be developed which states:

$$T = mU_E/g_C + (P_E - P_A) A_E \quad (1)$$

where

$$T = \text{thrust (lbf)}$$

$m$  = mass flow rate (lbm/sec)  
 $U_E$  = exit velocity (ft/sec)  
 $P_E$  = exit pressure (psi)  
 $P_A$  = ambient pressure (psi)  
 $A_E$  = nozzle exit area (inches squared)  
 $g_c$  = conversion factor  
= 32.2 (lbm-ft)/(lbf-seconds squared)

From this equation, it can be seen that thrust can be expressed as the sum of two factors. The first term, called the momentum flux, is the product of the propellant flow rate and the gas exhaust velocity relative to the vehicle. It comprises the largest part of the thrust and is caused by the momentum flux through the nozzle. Pressure thrust, the second term, is the product of the exhaust jet cross sectional area and the difference between the exhaust pressure and the ambient pressure. If the exhaust pressure is less than the surrounding pressure, the second term is negative producing a negative pressure thrust while an exit pressure greater than ambient yields a positive contribution to thrust. This second term is usually small compared to the momentum thrust, especially when the nozzle is operating near design conditions. Nozzles are often designed so the exit pressure is greater than or equal to ambient throughout most of its operating range (9:37).

The condition of exit pressure greater than ambient is called underexpansion since the flow exiting the nozzle is

capable of additional expansion (1:395; 4:410-412). This expansion takes place in the form of expansion waves causing the exhaust jet to expand outward from the nozzle. In this case, the pressure thrust contribution is positive. Should the expansion wave interact with a jet boundary, a system of alternating expansion and compression waves is formed as the fluid expands or compresses relative to ambient pressure. From this series of waves appears the familiar diamond pattern, seen in exhaust plumes of rocket engines, which dissipates the pressure mismatch between the engine exit plane and the surrounding ambient pressure (7:451-454). Once the expansion wave strikes a solid boundary, such as a nozzle shroud, it is reflected back as a compression wave. The compression wave, or oblique shock, turns the flow parallel to the original flow direction established prior to the expansion wave. This pattern of compression waves extends downstream in the jet exhaust flow and increases the exhaust fluid pressure as it passes through the compression waves. Conversely, a nozzle is said to be overexpanded if the ambient pressure is greater than the nozzle exit pressure. The pressure thrust term is negative and the diamond pattern system starts with an oblique shock (compression wave) to accomplish the pressure difference dissipation. A third case occurs whenever the nozzle exit pressure is equal to the ambient pressure. This is called a perfectly expanded condition and exists at one ambient pressure (the design altitude) resulting in neither expansion nor contraction of

the exhaust jet.

Clustering unshrouded rocket nozzles often results in an increase in thrust. Goethert (4:12) noted that pressure higher than the ambient pressure was trapped in the confined space between clustered nozzles by the interaction of the individual nozzle exhaust flows. This higher pressure creates a positive pressure thrust contribution applied at the base of the rocket vehicle.

Adding shrouds to a clustered nozzle arrangement may produce a larger effective jet exhaust area. If the underexpanded flow attaches to the shroud the pressure thrust term will be determined by the increased exit area and the pressure that occurs at the exit plane of the assembly. This larger area affects the nozzle performance characteristics by changing the exit Mach number, the assembly exit to throat area ratio, and the combustion chamber to exit plane pressure ratio and therefore the momentum thrust term. Examples of the various flow regimes can be seen in Figure 1 (3:8) which shows nozzle pressure ratio versus varying nozzle exit to throat area ratios.

### Objectives

Previous AFIT thesis work by Moran (8) and Bjurstrom (2) studied the effects of clustering rocket nozzles with and without shrouds respectively. In this project, the experimental apparatus was established to examine clustered

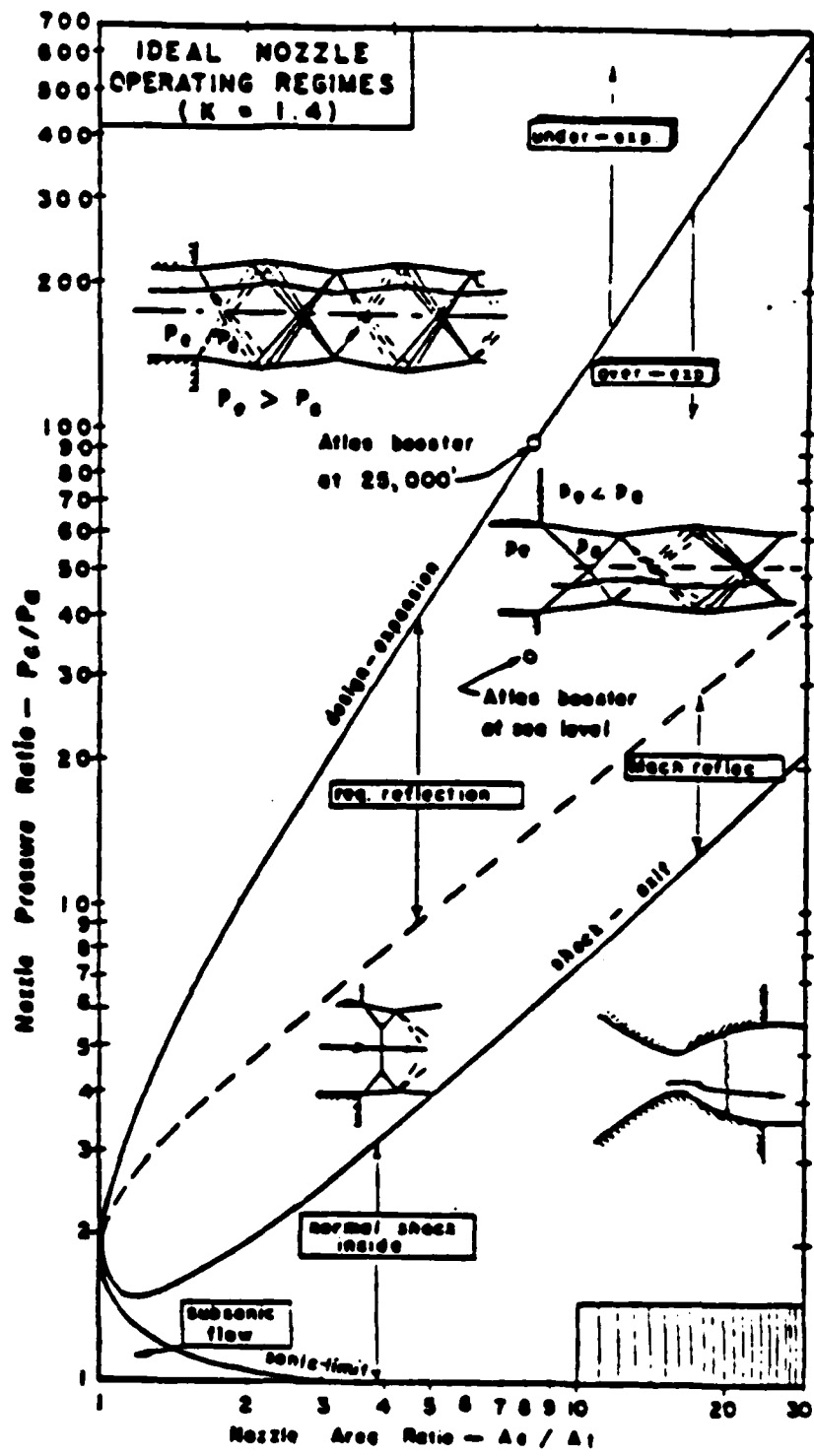


FIGURE 1. NOZZLE OPERATING DIAGRAM (3:8)

nozzles with and without shrouds under high altitude conditions with these specific objectives:

1. To experimentally analyze the effect of shrouds on the exit base pressure of clustered nozzles and the pressure distribution along the shroud walls.

2. To improve the experimental apparatus in order to facilitate model changes.

## II EXPERIMENTAL APPARATUS

This experimentation was accomplished using the AFIT blowdown wind tunnel. Laboratory air at 100 psig and 75 degrees Fahrenheit was supplied to the test section through a stilling chamber. Evacuating a 535 cubic foot vacuum chamber to 0.30 psia established a pressure ratio up to 400 across the scale model clustered rocket nozzle assembly. The vacuum facility could not maintain the pressure ratio during the test run so the pressure ratio decrease simulated operating the nozzle assembly at decreasing altitudes as the experiment proceeded. Increasing vacuum chamber pressure with run time was seen as increased back pressure on the nozzle assembly. The test section was installed in an intermediate vacuum chamber (Figure 2) equipped with windows to permit the use of flow visualization techniques for studying the flow. The equipment was designed to accommodate a variety of nozzle blocks and shroud lengths. By changing nozzle blocks and shrouds, many possible configurations could be simulated. Also, the addition of an instrumentation collar simplified changes in the test articles. Test articles investigated included two- and three-dimensional nozzle blocks with one to four convergent-divergent nozzles and with two nozzle shroud lengths. An automatic data acquisition and reduction system, described in Chapter III, was used to record and reduce all data.

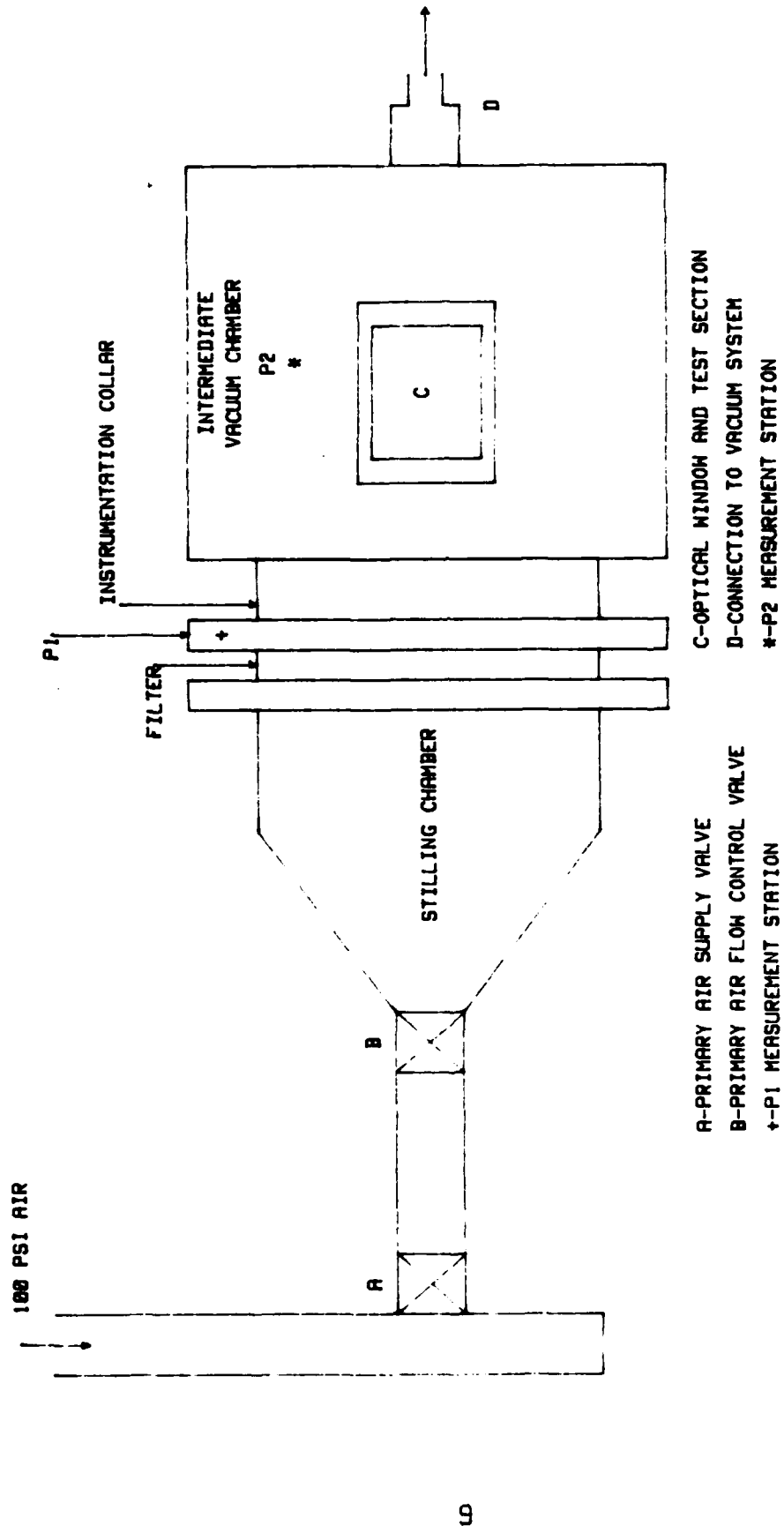


FIGURE 2. SYSTEM SCHEMATIC

## Flow System

Compressed air at 100 psig was supplied by a 100 hp compressor through a three inch line (Figure 2). A hand operated fast opening gate valve controlled the flow into the stilling chamber, insuring a uniform flow through the test section. One additional valve, downstream of the gate valve, provided a means of controlling the air pressure in the test section. The test section was placed in the intermediate vacuum chamber attached to the vacuum system. Ten inch square optical quality viewing ports were fitted in this chamber allowing still photographs and 16mm filming of the flow passing through the nozzles with flow visualization using Schlieren apparatus. A paper filter mounted upstream of the test section removed moisture droplets and particles from the flowing air.

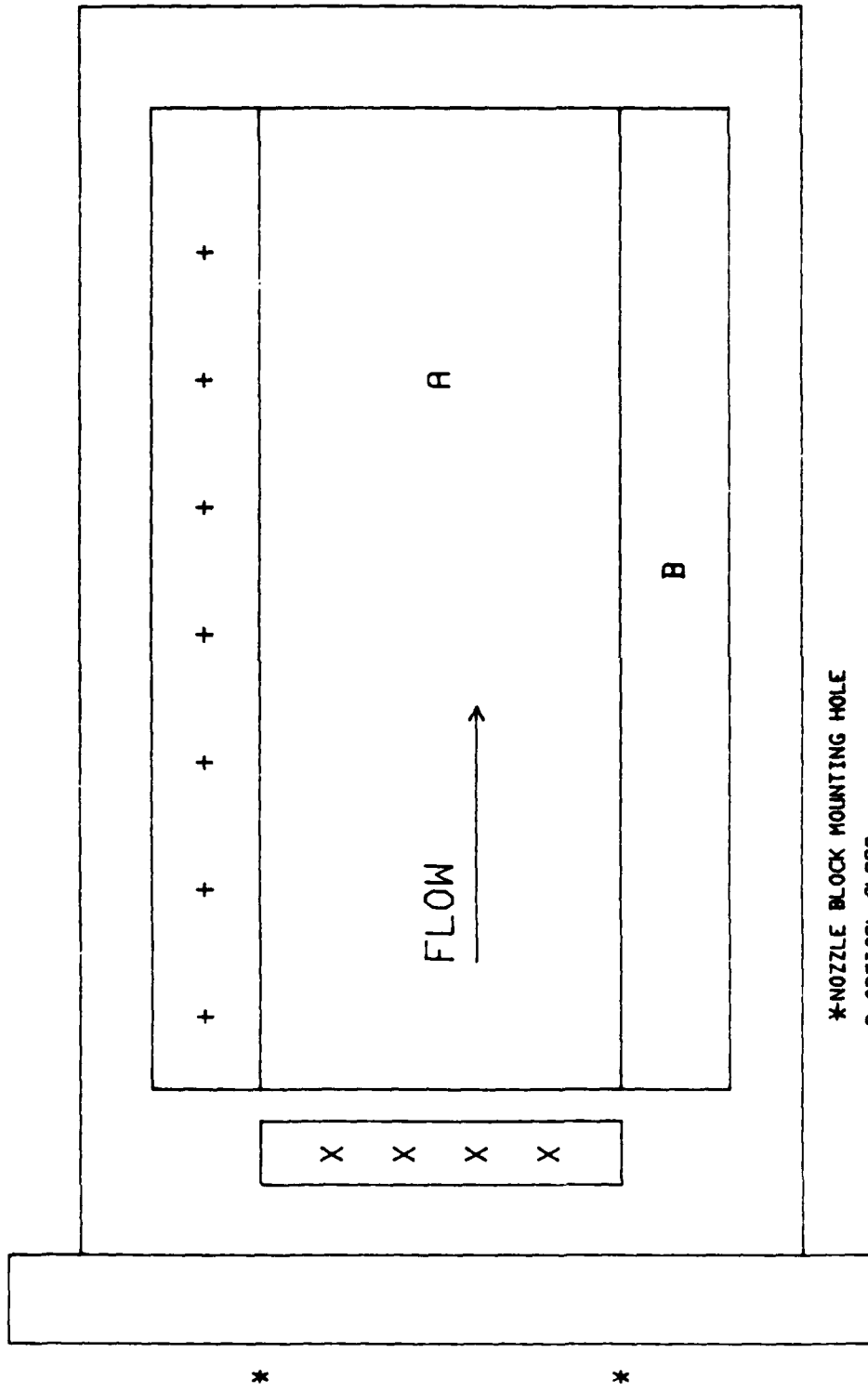
## Instrumentation Collar

The instrumentation collar (Figure 2) was added to the apparatus in order to improve model change capability and reduce the time required for this change. Before the addition of the collar, each change required removal of all external transducer and vacuum connections prior to separating the stilling chamber from the vacuum chamber. With the collar in place, the chambers could be separated without removing any of the connections, reducing model change time.

The instrumentation collar is a three and one half inch wide aluminum collar mounted on the large end of the stilling chamber. It is circular in shape (with a 16 inch outer diameter and 12 inch inner diameter) and sized to fit within the chamber closure bolts. All of the transducer wiring and vacuum hoses pass through fittings in the collar and attach to the test section. The collar provided easy access to the model when the stilling chamber/collar combination was separated from the vacuum chamber. Twelve milled flats on the outer circumference, two used in this investigation, provide room for future growth in instrumentation requirements.

#### Test Section

The test section (Figure 3) consisted of a nozzle block and a flow channel mounted on the instrumentation collar. The nozzle blocks were inserted into the test section with the sides of the section acting as the shrouds sidewalls. Optical glass was used for the sides allowing for Schlieren photographs. The wooden top and bottom shrouds, with lengths of 3 and 8 inches, were removable so various shroud lengths could be investigated. They were designed so pressure measurements could be made along the surfaces exposed to the main air flow by mounting transducers in the shrouds. The shroud transducers were numbered with the lowest number closest to the nozzle block and the numbers ascending towards



\*NOZZLE BLOCK MOUNTING HOLE

A-OPTICAL GLASS

B-BOTTOM SHROUD

+--TOP SHROUD TRANSDUCER MOUNTING HOLES

X-NOZZLE BLOCK TRANSDUCER MOUNTING HOLES

FIG. 3. TEST SECTION

the end of the test section.

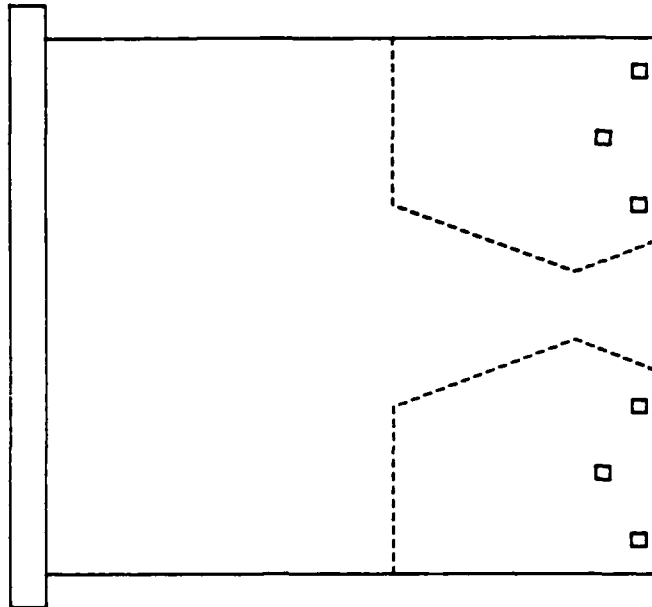
### Nozzle Blocks

Four nozzle blocks were used. Block 1 had a single nozzle while Block 2 had three nozzles as seen in Figures 4 and 5 respectively. Their exit to throat area ratio (AR) was 8:1 yielding an exit Mach number of 3.68. Block 3 (Figure 6) was similar to Block 1 except the area ratio was 4:1 and the resultant Mach number 2.94. One three-dimensional nozzle block (Block 4) was used. Block 4 had an area ratio of 3:1 and Mach number of 2.64 (Figure 7). All blocks had pressure transducer mounting holes at locations shown in Figures 4-7. The pressure measurement stations were numbered from top to bottom except for Block 4 which was numbered with the center station P3, the top P5, and the bottom P4 because of wiring requirements (Figure 7).

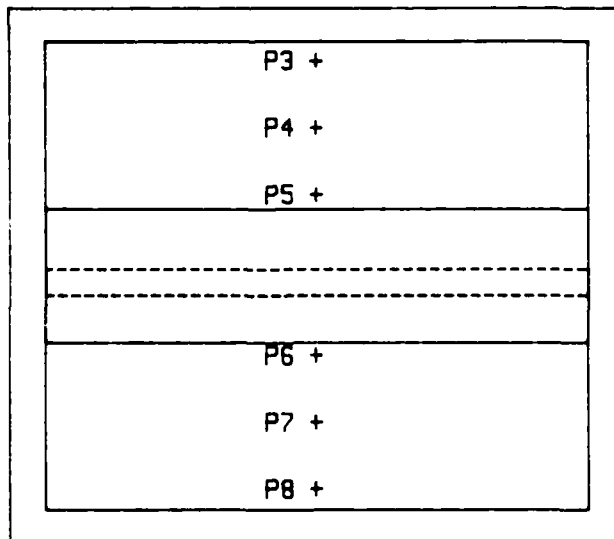
### Configurations

To identify each combination of nozzle blocks and shrouds, a system of configurations was established. These configurations, designated by a number/letter combination, identified the data from each test run and determined the number of transducers used in each model. The number signified the nozzle block used and the letter represented the shroud length. The configuration designators along with

SIDE VIEW



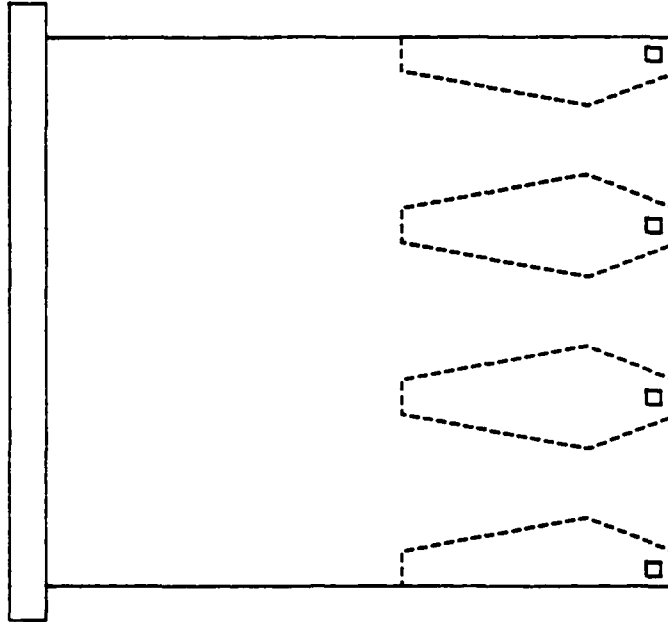
FRONT VIEW



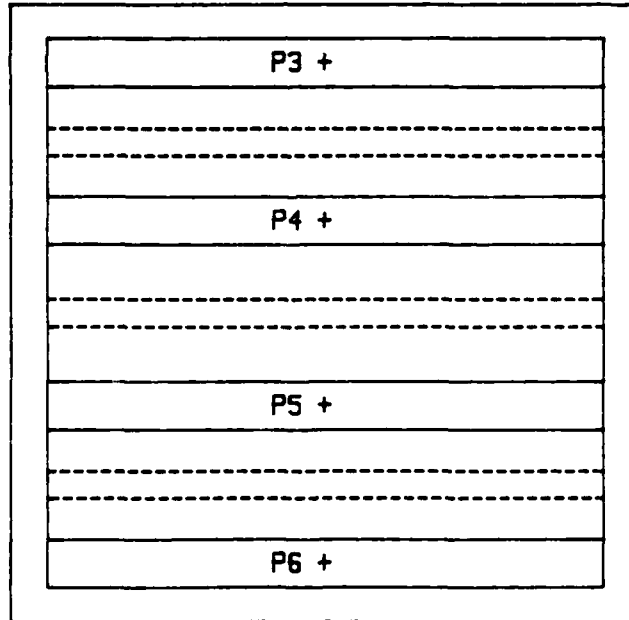
□ - TRANSDUCER MOUNTS  
+ - MEASUREMENT STATIONS

FIGURE 4. NOZZLE BLOCK 1 (AR=8:1)

SIDE VIEW



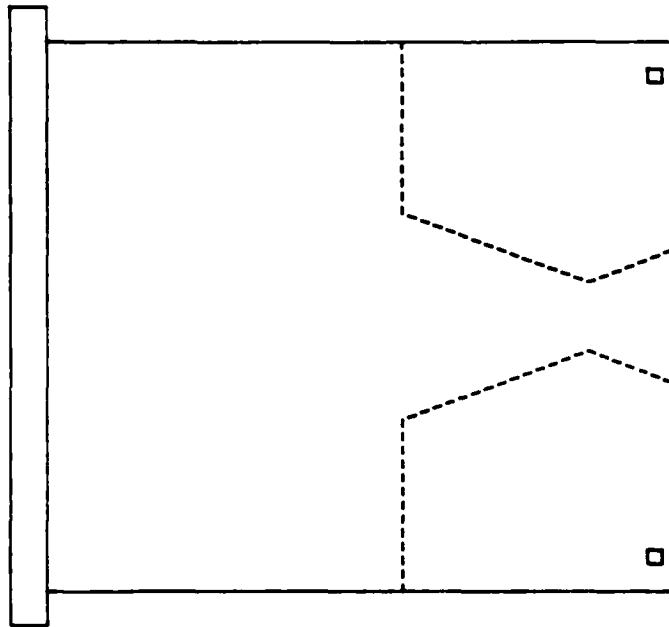
FRONT VIEW



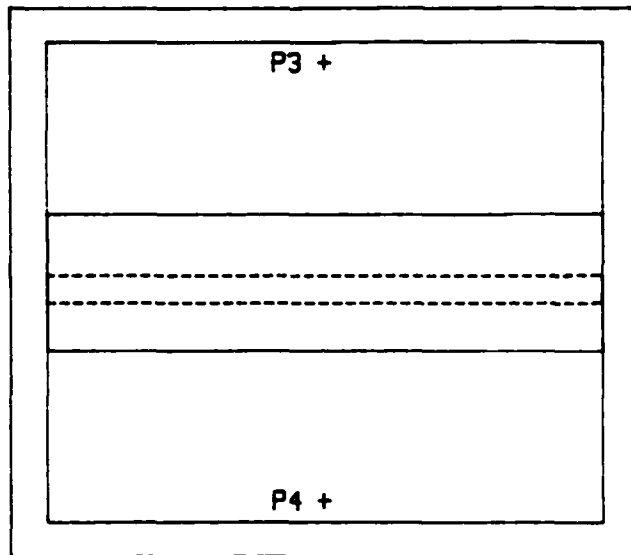
- - TRANSDUCER MOUNTS
- + - MEASUREMENT STATIONS

FIGURE 5. NOZZLE BLOCK 2 (AR=8:1)

SIDE VIEW



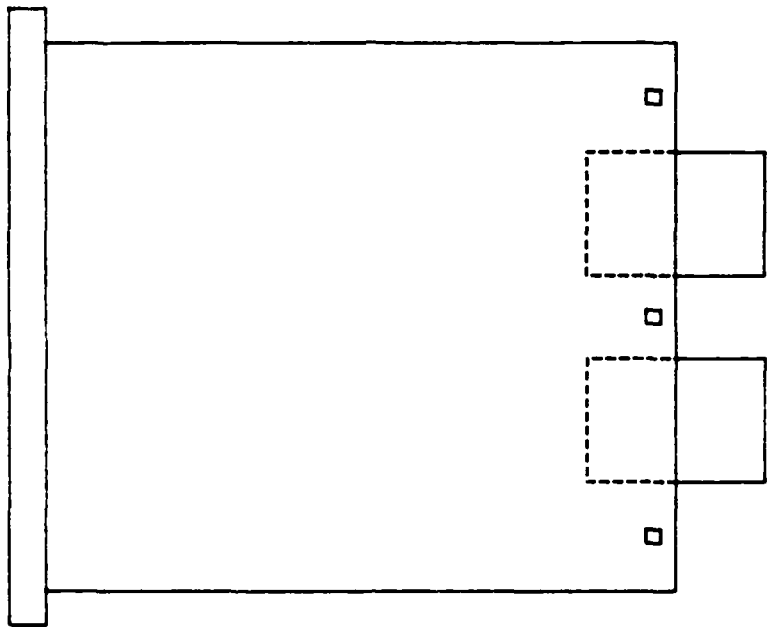
FRONT VIEW



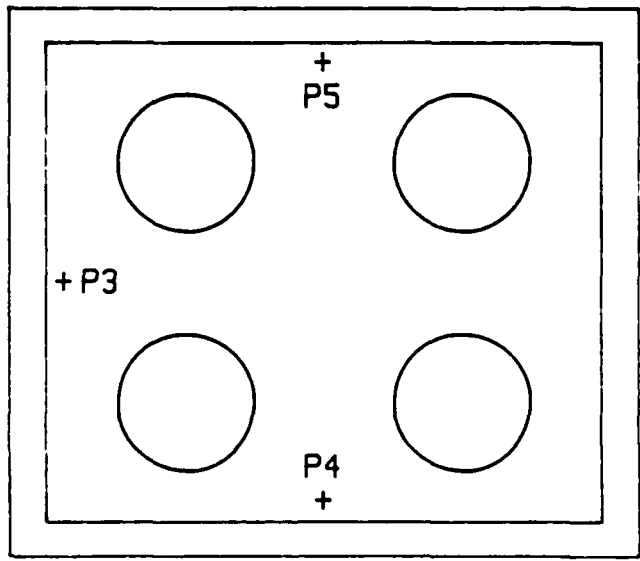
- -TRANSDUCER MOUNTS
- + -MEASUREMENT STATIONS

FIGURE 6. NOZZLE BLOCK 3 (AR=4:1)

SIDE VIEW



FRONT VIEW



- -TRANSDUCER MOUNTS
- + -MEASUREMENT STATIONS

FIGURE 7. NOZZLE BLOCK 4 (AR=3:1)

the shroud length and number and location of each model's transducers can be seen in Table I.

### Instrumentation

Fourteen piezoresistive pressure transducers were used to record data. The upstream pressure (P1) was measured by an Endevco 8530A 0-100 psia transducer. It was located on the instrumentation collar downstream of the paper filter (Figure 1). The downstream or back pressure (P2) was measured by a Bell and Howell 0-5 psia transducer located downstream of the test section in the intermediate vacuum chamber. Base pressure on the nozzle blocks was recorded using Endevco 8510B 0-5 psid transducers. All pressure measurements along the shroud were accomplished with Endevco 8506B 0-5 psid transducers mounted in the top shroud (Figure 3). The short shroud length required three and the long shroud six transducers for proper coverage. Shroud transducer numbering was dependent upon the nozzle block/shroud combination.

The Endevco psid transducers in this experiment were used to measure absolute pressure (psia). They are capable of measuring static or dynamic pressures and either gauge or differential pressure depending upon the reference pressure used. A near absolute vacuum was connected to the rear face of each transducer diaphragm through a tube vent. This vacuum became the reference which the pressure acting on the external side of the diaphragm was compared with. This, in

Table I Configurations

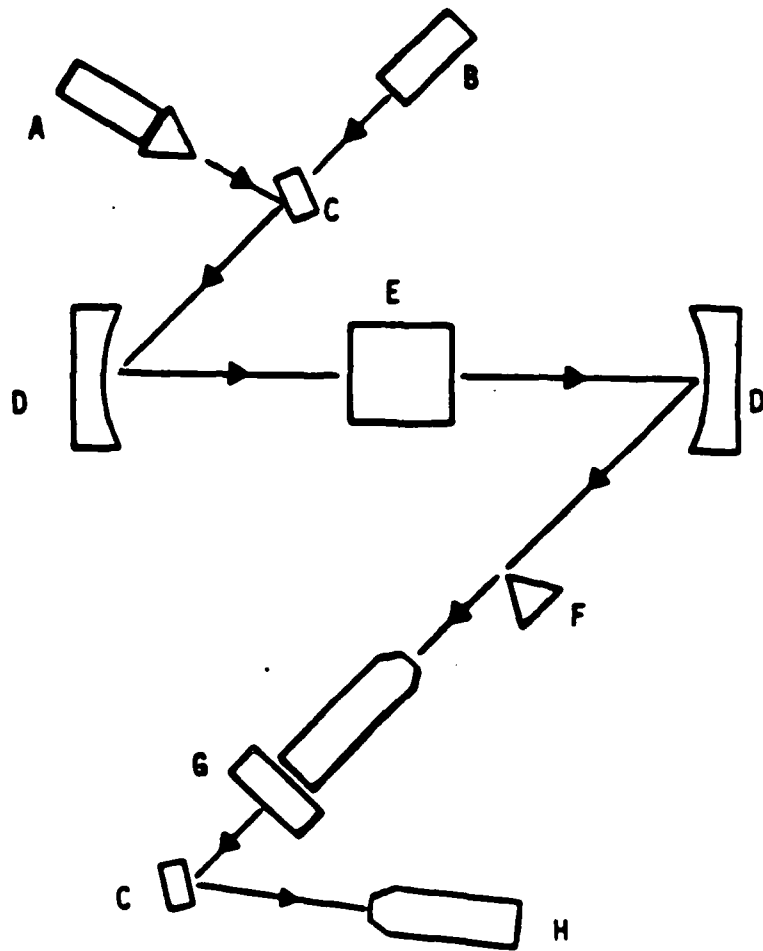
<u>Configuration Number</u>	<u>Shroud Length (inches)</u>	<u>Nozzle Block Transducers</u>	<u>Shroud Transducers</u>
1A	3	P3-P8	P9-P11
1B	8	P3-P8	P9-P14
1C	0	P3-P8	none
2A	3	P3-P6	P7-P9
2B	8	P3-P6	P7-P12
3A	3	P3-P4	P5-P7
3B	8	P3-P4	P5-P10
3C	0	P3-P4	none
4A	3	P3-P5	P6-P8
4B	8	P3-P5	P6-P11
4C	0	P3-P5	none

effect, changed the measurement scale to absolute pressures.

In addition to the transducers, two mercury manometers were used during the test and calibration runs. The first was connected to the vacuum chamber, and the second to the transducer vacuum reference pump. A precision pressure gauge, model FA160, was also attached to the reference pump to insure that a near absolute zero reference was attained. The vacuum chamber manometer was used to monitor the ambient conditions in the vacuum tank prior to the test run. To facilitate transducer calibration, a 0.25 inch outside diameter line was connected from the 100 psig air supply through a small valve into the stilling chamber. This permitted incremental adjustment of chamber pressure during calibration.

#### Schlieren System

One of the goals of this experiment was to determine the nozzle-exhaust flow patterns as conditions changed from underexpanded to overexpanded flow regimes. For this, a Schlieren system was used allowing still pictures as well as motion pictures. Polaroid sheet film, used in conjunction with a spark lamp, provided the still pictures. By using a steady lamp, the flow conditions could be viewed on a flat mirror used in place of the still camera. The photographs were used to supplement pressure transducer data. Figure 8 shows a typical Schlieren system.



- A. Steady light source (motion pictures)
- B. Spark lamp (still photos)
- C. Flat mirror
- D. Concave mirror
- E. Test section
- F. Knife edge
- G. Still camera (still photos)
- H. Film or video camera (motion pictures)

FIGURE 8. SCHLIEREN SYSTEM (6:13)

### III DATA ACQUISITION AND REDUCTION SYSTEM

A Hewlett Packard (HP) 6901S Measurement and Analysis System was used to collect the raw data from the transducers and reduce it to a usable form. The experimental apparatus was designed to interface with the HP6901S using the hardware components listed in Table II. These components were interconnected as shown in Figure 9. All of the hardware pieces were linked using the HP-IB interface bus. The HP-IB allows the connection of several external devices, such as printers, plotters, and disk drives to the computer and can be thought of as a centralized coordination center. It can selectively send data to the individual devices and tailors the data flow rate to the requirements of each receiving device. Data flow to the computer from the external devices can also be controlled by the bus.

The HP6901S provides a multiple channel data acquisition and reduction capability. It can collect up to 264 channels of either analog or digital data, with a total collection capability of 4096 samples. With the full complement of sixteen interface cards, a sample rate of 100,000 samples per second is possible. This investigation, however, did not require the full sampling capability of the system. Figure 10 is a simplified diagram of how the HP6901S interfaces with the other operational devices.

The HP6901S is designed to have an HP6942

Table II Test Instrumentation

<u>Item</u>	<u>Model #</u>	<u>Serial #</u>
Pressure Transducer(P1)	Endevco 8530	39BP
Pressure Transducer(P2)	Bell and Howell	5321
Pressure Transducer(P3)	Endevco 8510	80HB
Pressure Transducer(P4)	Endevco 8510	79HB
Pressure Transducer(P5)	Endevco 8510	78HB
Pressure Transducer(P6)	Endevco 8510	90EK
Pressure Transducer(P7)	Endevco 8510	87EK
Pressure Transducer(P8)	Endevco 8510	PP81
Pressure Transducer(P9)	Endevco 8506	74BF
Pressure Transducer(P10)	Endevco 8506	68BF
Pressure Transducer(P11)	Endevco 8506	86BF
Pressure Transducer(P12)	Endevco 8506	97BF
Pressure Transducer(P13)	Endevco 8506	82BF
Pressure Transducer(P14)	Endevco 8506	83BF
Power Supply	HP6205C	2208A-00631
Multiprogrammer	HP6942A	2513A-06003
Computer	HP9826	2313A05860
Plotter	HP7470A	97468
Printer	HP2934A	2635A32528
Measurement and Analysis System	HP6901S	234A00104
Portable Vacuum Standard	PV2-2A-10000	44362-1

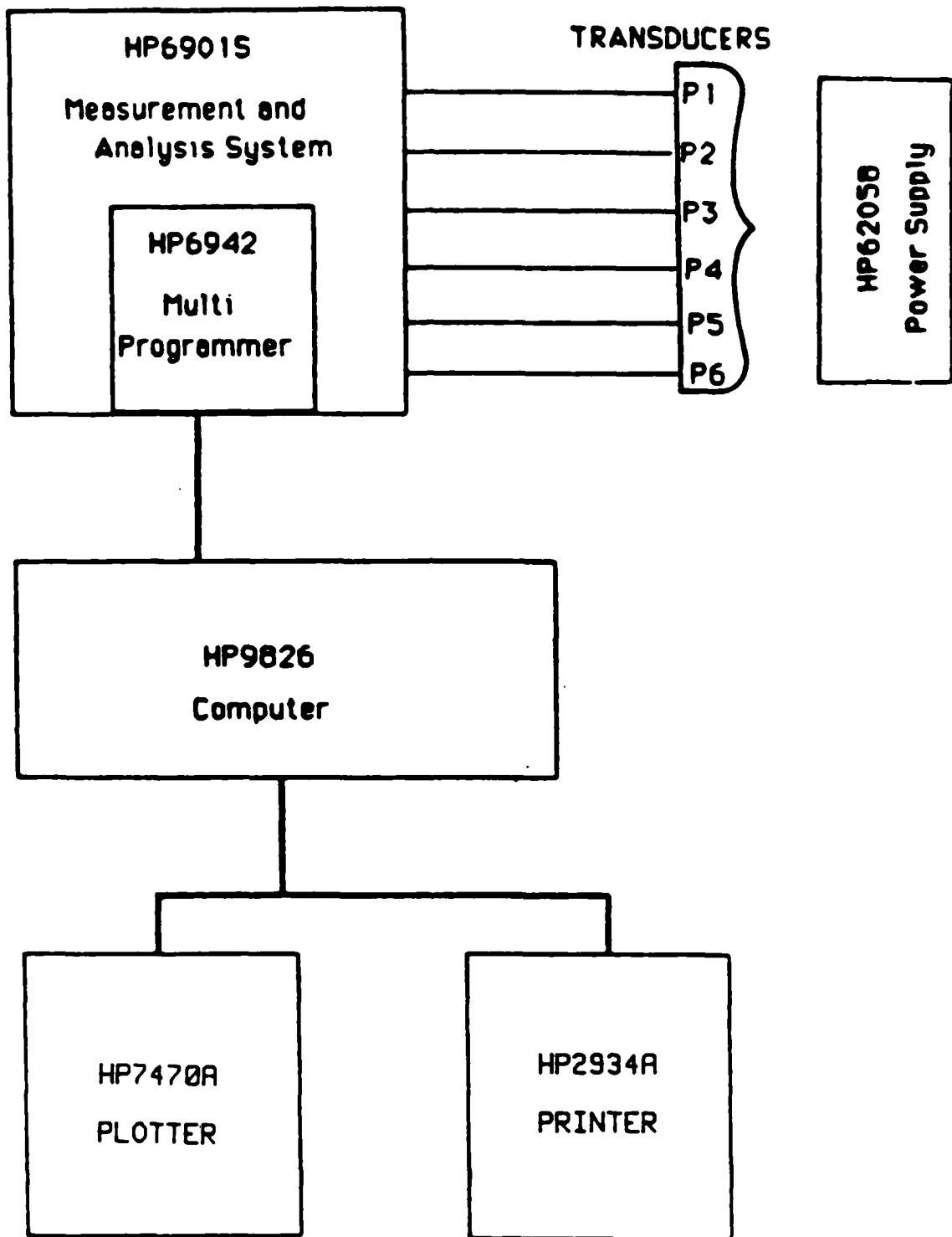


FIGURE 9. HARDWARE SCHEMATIC (8:16)

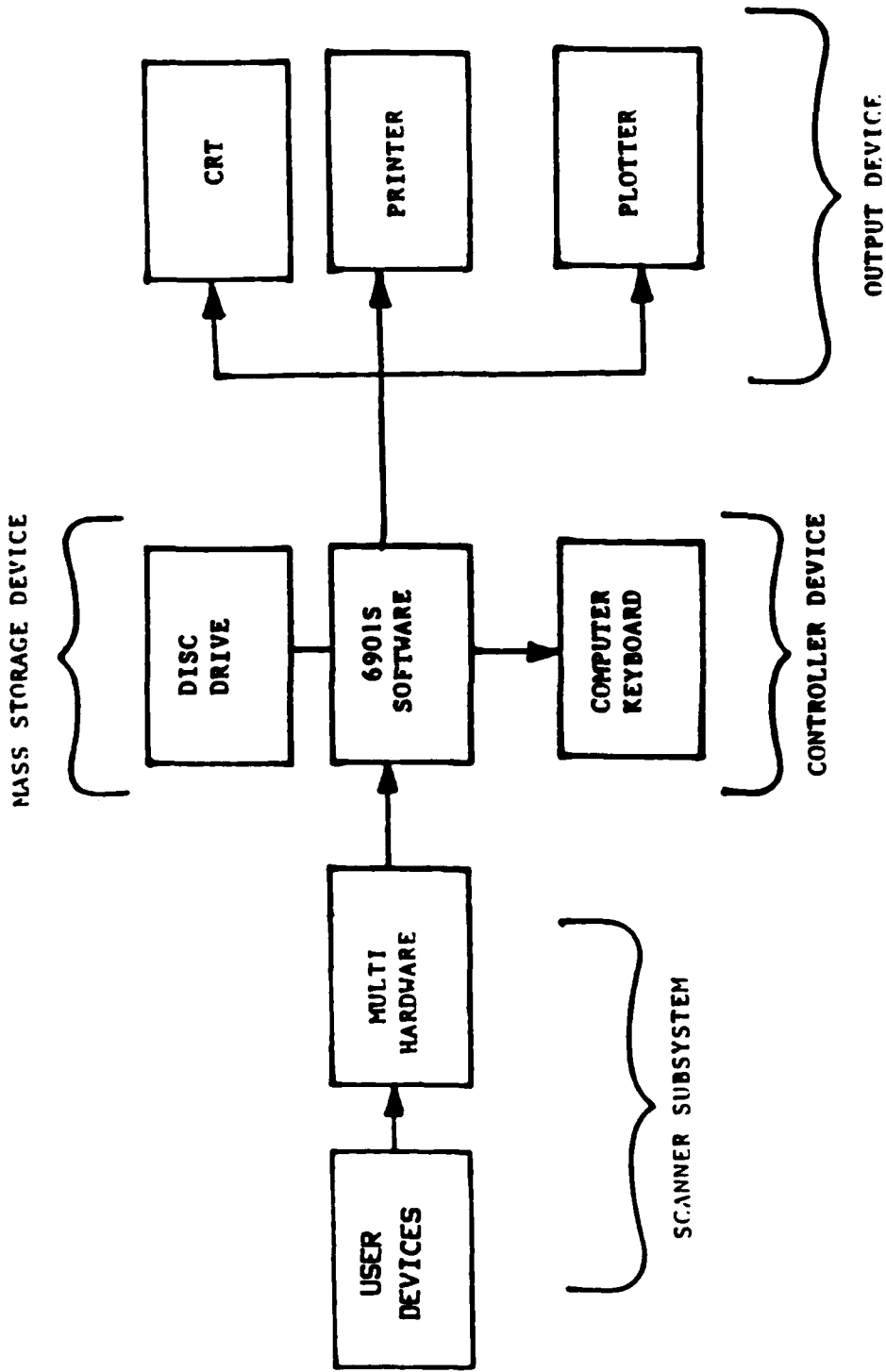


FIGURE 10. SIMPLIFIED HP6901S SYSTEM (8:17)

Multiprogrammer mounted internally. The HP6942 contains the memory cards, analog to digital converters, scanner relays, and controller cards required for system operation. Data is acquired through the HP6901S terminal boards and temporarily stored. This storage is required in order to achieve the desired sampling rate while not overloading the analog to digital conversion capability. The data is then recalled from storage in sequential order, converted to digital form, and sent to the HP9826 computer for storage on floppy disk. Figure 11 shows the general data flow.

The HP9826 computer and HP6901S are menu driven systems (Figure 12). The menus are executable from the keyboard and provide the means for entering experimental parameters. The test run data acquisition parameters including sample rate, number of samples and the method of triggering the data acquisition, were entered using HP6901S software. For this study, the software was set to sample all channels every 0.11 seconds with an interval of 8000 microseconds between each successive channel. Total run time was between 30 and 40 seconds for all data runs. The software package also provided several data presentation options such as tables, graphs, or histograms. The data reduction process, with appropriate offset values inserted to scale the data, was accomplished prior to receiving the selected output presentation.

Several programs were written to obtain the desired hard copy graphical output. These plotting programs load the data

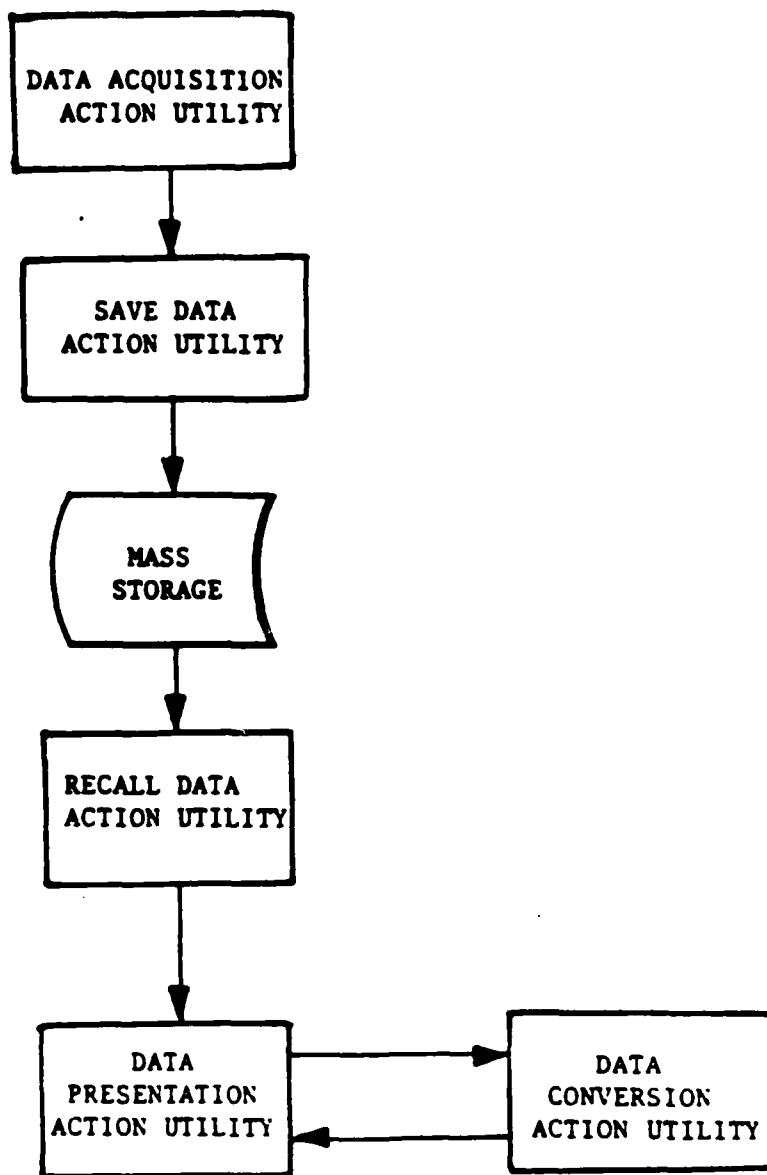


FIGURE 11. DATA FLOW PATH (8:19)

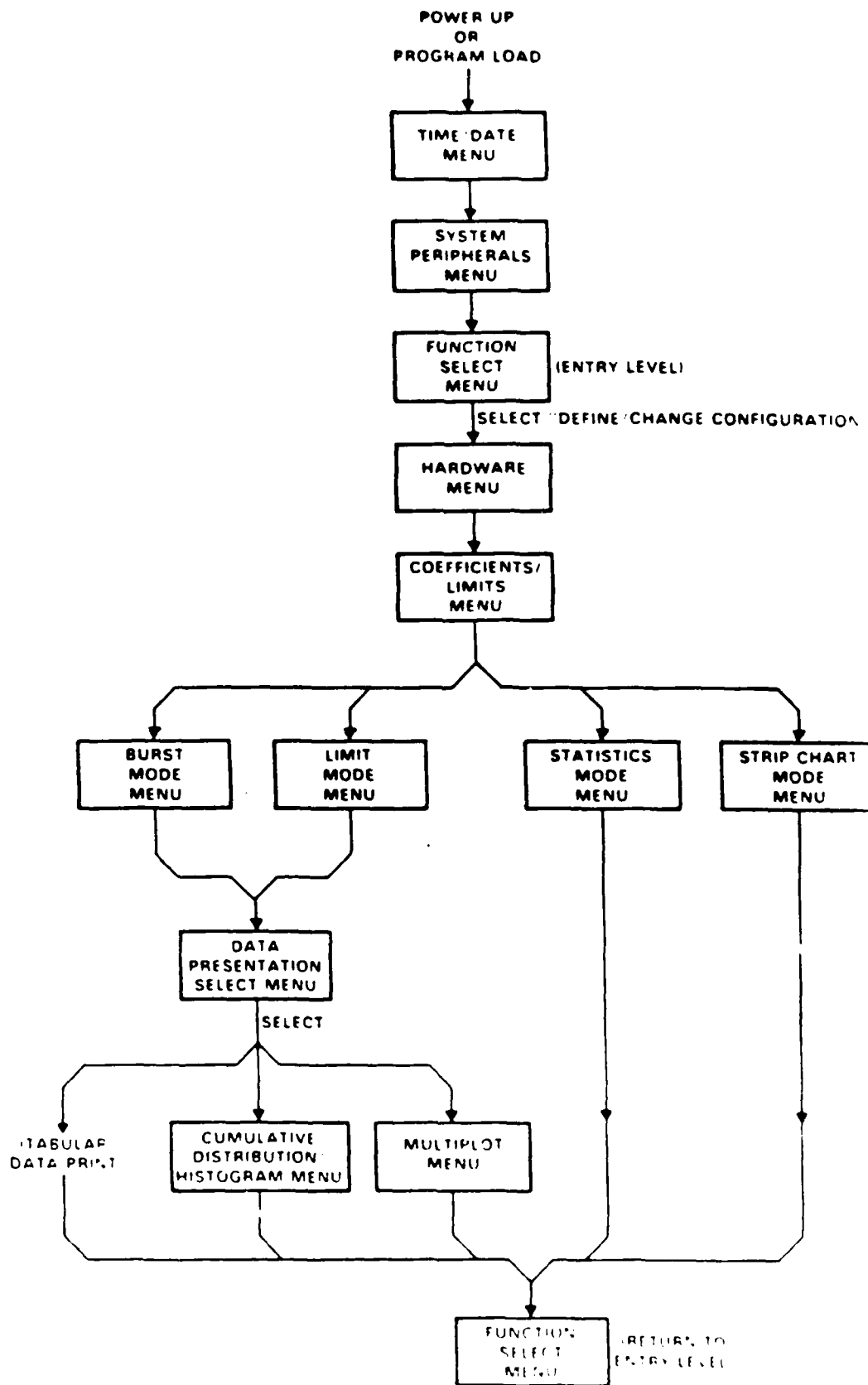


FIGURE 12. OPERATIONAL FLOW OF HP6901S MENU UTILITIES

file by assigning I/O paths to refile the transformed data for plotting on the HP7470A plotter. In addition, they were modified so that graphs of pressure versus pressure ratio could be obtained. This removed time as a variable and negated the effect of the particular apparatus on the data presentations. Flexibility was built into the programs to allow for other alternatives of graphical presentation.

The data acquisition and reduction system was suitable for research using the blowdown facility. The pressure characteristics of the nozzle blocks and shrouds were adequately acquired, processed, and formatted. This system is expandable and easily adaptable for future research. Should future work require more complex computations, a Fortran or Pascal compiler should be added to improve numerical computational ability by reducing the time required to perform the computations.

#### IV EXPERIMENTAL PROCEDURES

##### Calibration

All of the Endevco 8510, 8506, and 8530 pressure transducers were calibrated using the MKS Portable Vacuum Standard (PVS). The PVS provided a reference pressure for the transducer. This reference was compared to an outside air pressure source acting on the measurement face of the transducer, producing a voltage differential. The voltage generated from this differential was recorded, along with the pressure differential, on a digital voltmeter and the transducer sensitivity then calculated from the slope of the pressure versus voltage curves.

The back pressure transducer (P2) was calibrated in place on the apparatus. This transducer measured absolute pressure (psia) so no separate vacuum reference was required. The tank pressure was first lowered to the initial operating conditions of 0.30 psia as measured by the mercury manometer connected to the vacuum tank. The pressure was then varied by using a small valve opening to the atmosphere. As the pressure changed, the voltage was recorded on the voltmeter and plotted versus pressure to determine transducer sensitivity. All the transducers were connected to a 10 volt power supply during testing and calibration.

## Test Procedure

The test procedure was the same for all test runs. First, the valve controlling the 100 psig air into the stilling chamber was closed. Then the main air supply valve was opened allowing the 100 psig air to flow into the supply tube. The transducer vacuum reference pump was turned on next. This pump, producing near absolute zero as a reference, made the Endevco 8510 and 8506 transducers, in effect, absolute pressure transducers. All of the associated electronic equipment for the transducers was turned on in order to warm up and the power supply voltage was set to 10 volts. The instrumentation amplifier (Figure 13) converted the two wire transducer output into a one wire output suitable for HP6901S Measurement and Analysis System input. The amplifier was adjusted so the voltage entering and exiting was equal to the transducer output voltage. The mode rejection ratio characteristics of this amplifier preserved the signal while producing a cleaner transducer output. The HP6942A multiprogrammer and computer system were turned on and the data acquisition and reduction programs loaded. Next, the two main vacuum pumps were used to set the initial operating conditions. Since the downstream pressure varied continuously during a test run, the lowest possible back pressure was established before each run. Because of small leaks in the vacuum system, the initial value was limited to around 0.30 psia.

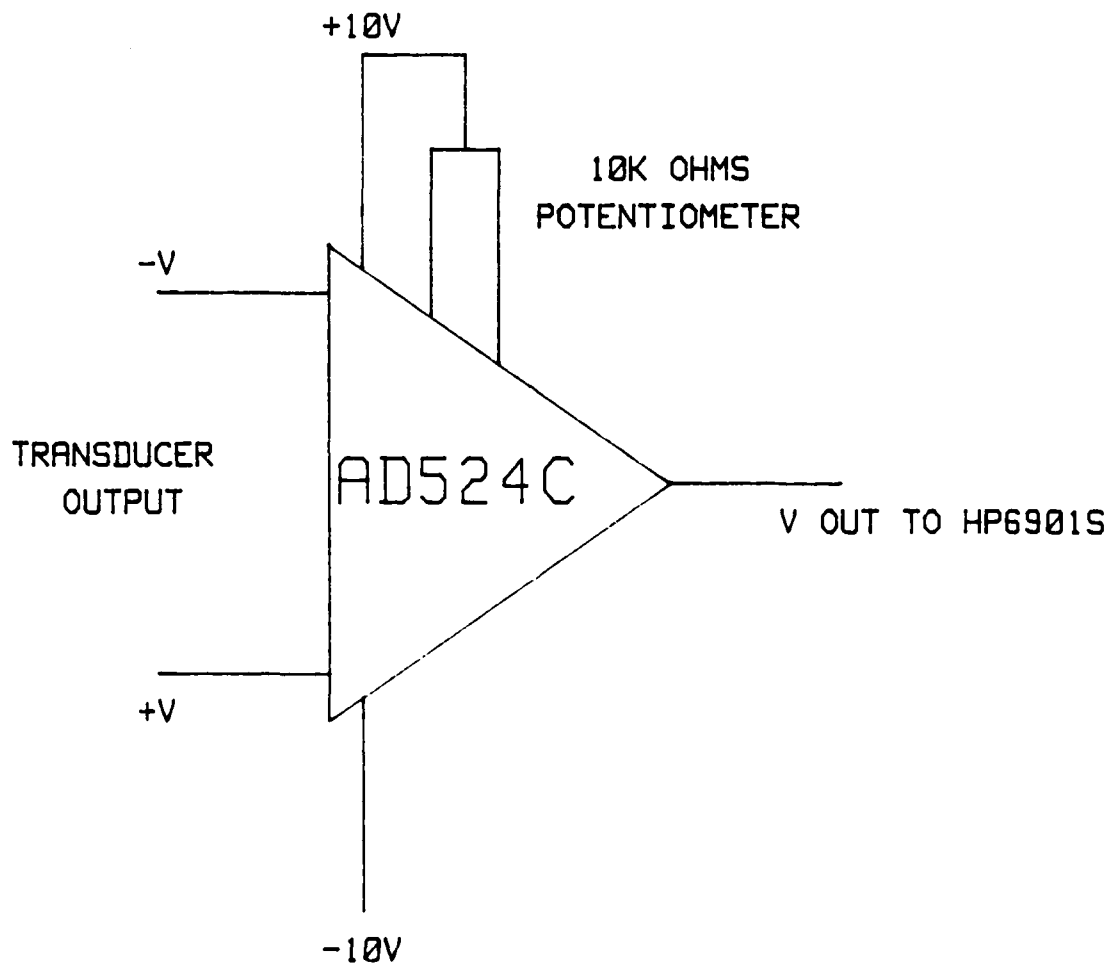


FIGURE 13. INSTRUMENTATION AMPLIFIER

Once the initial conditions were established, the test run was started. At the commanded point in the data acquisition program, the gate valve was opened allowing air into the stilling chamber/vacuum tank. After completing the desired test time, the valve was closed cutting off the air flow. The computer stored the data and reduced it to pressure versus time data by using the computed transducer sensitivities.

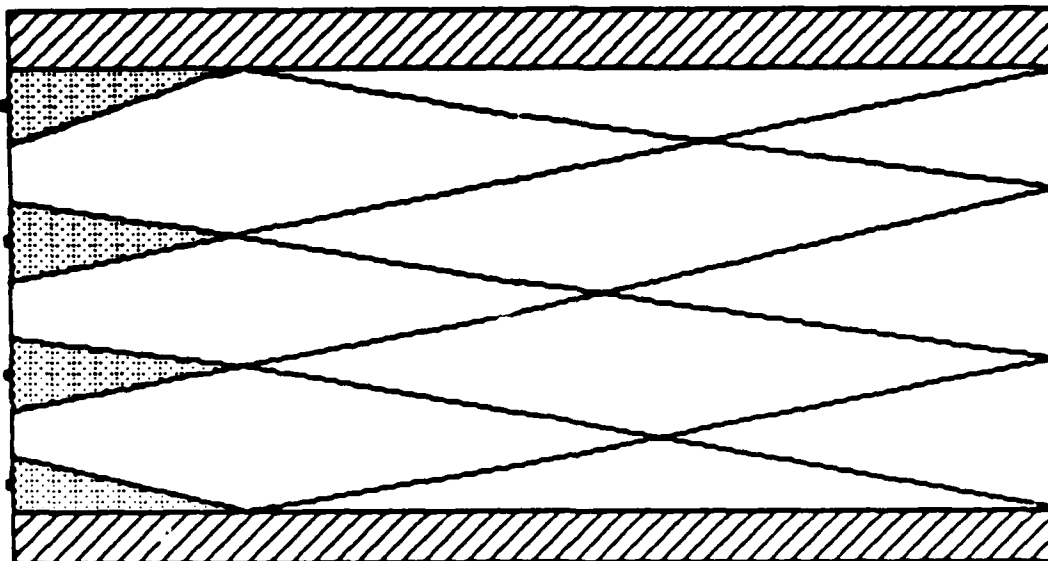
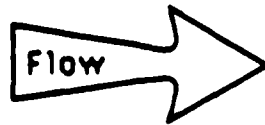
Data from the pressure transducers were recorded with the HP6901S and the HP9826 for several test runs with each nozzle configuration. These runs were made at different starting back pressures to demonstrate that there were no prior history effects. In other words, flow condition changes occurred at the same nozzle inlet to ambient back pressure ratio no matter what the starting condition. The vacuum system was not capable of providing increasing pressure ratios during a run and therefore could not be used to check for hysteresis. An improved vacuum system capable of steady state conditions would greatly improve the research accomplished on this facility. By being able to evaluate increasing pressure ratios, simulating a boost vehicle's ascent, a researcher could better model an actual nozzle assembly's performance and insure that test results are a function of pressure ratios and not affected by hysteresis.

## V RESULTS AND DISCUSSION

The exhaust behavior of a single supersonic nozzle in the underexpanded and overexpanded flow regimes has been well established (5:410-412). When two or more nozzles are operating close together (as well as a single nozzle) in a shroud, additional effects are created by the flow attachment to the shroud and the interaction of the jet exhausts.

Since the shrouded nozzle sees a larger effective nozzle expansion ratio, exit area to throat area, the momentum thrust term (Equation 1) is increased. Study of Schlieren photography shows that flow expands coming out of the nozzle until it attaches to the shroud. This attached flow affects the pressure distribution along the nozzle exit plane and the shroud walls. Low pressure is trapped along the nozzle base and along the shroud walls by a system of compression waves created when the expansion wave reflects off the shroud wall. This system of waves isolates the base area and shroud walls from the ambient conditions. Figure 14 shows a simplified drawing of the isolated base plate areas and the resulting system of compression waves. Holmes and Matz (6:15) stated the higher shroud wall pressures resulted from the jet on jet and jet on wall recompression systems generated by the exhaust flow expansions since the compression waves turned the flow with a corresponding increase in static pressure.

An ascending rocket transitions from high ambient sea level conditions to near absolute vacuum during its flight.



■ Base plate areas isolated from the backpressure by the flow expanding to the shroud

▨ Shroud

\* Nozzle exit plane

FIGURE 14. BASE PLATE AND CHANNEL FLOW (8:29)

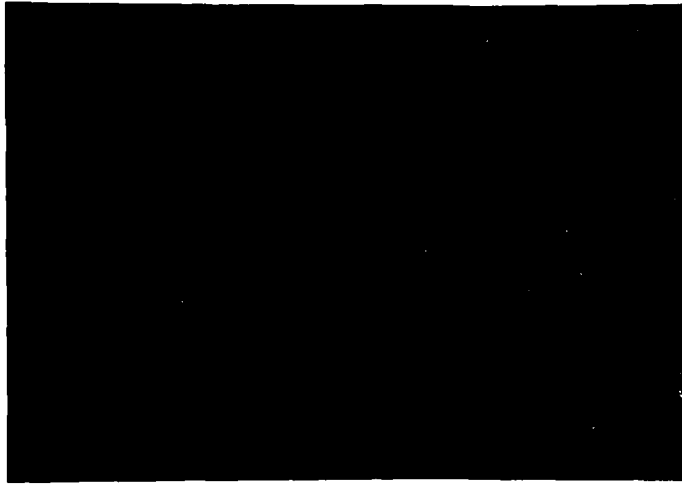
In this investigation, the nozzle inlet to ambient back pressure ratio change is reversed from that of a rocket vehicle booster. Initially, the ambient back pressure is much lower than the nozzle upstream pressure and gradually increases during the test run. Because of the symmetry of the nozzle block and shroud configuration, the experimental results were the same on the top and bottom halves. Comments will refer only to the top half with the understanding that it applies equally well to the bottom half.

The flow began with the nozzle in an underexpanded condition so the jet attached to the shroud and the exhaust plumes of the multiple nozzle block interacted. Normally, an ascending rocket would not transition to this phase until passing the nozzle design altitude, which would be approximately 61,000 feet for the nozzles used in this experiment. The flow expansion outside the rocket nozzle resulting in attachment to the shroud walls produces a system of compression waves which isolates the nozzle exit plane and the shroud walls from the ambient pressure. Additionally, the compression system raised the flow field pressure inside the shroud as the flow moved downstream. If this compression system extends the length of the shroud, the complete shroud and nozzle system can be considered started. When this is true, the shroud exit pressure may be greater than the ambient back pressure. The duration and type of isolation was dependent upon system geometry and the nozzle inlet to ambient back pressure ratio. The pressure measured by the

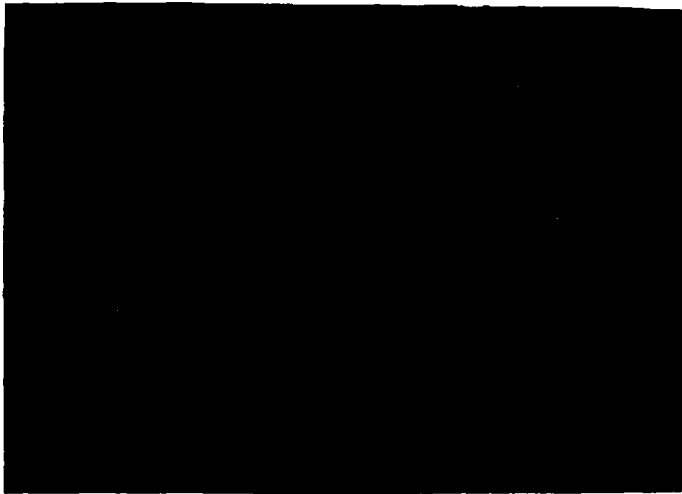
various transducers versus the nozzle inlet to ambient pressure ratio histories and the Schlieren photographs can be found in Appendices A and B. Appendix A contains the plots and photographs from the base exit pressure measurements and Appendix B from the shroud measurements.

### Base Pressures

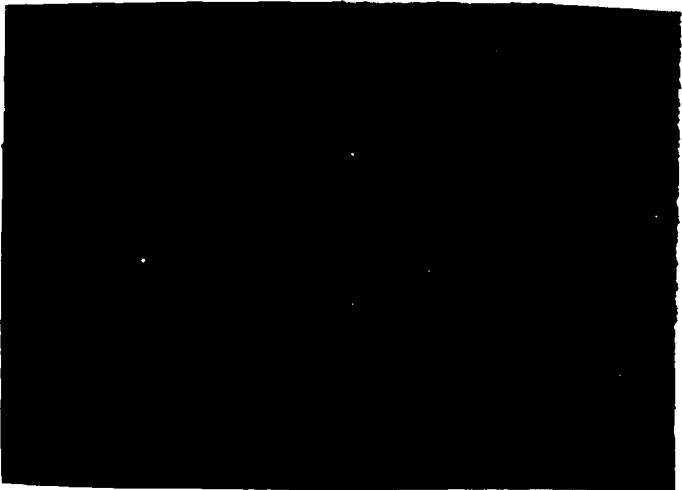
The flow of configuration 1A (Con1A) was initially underexpanded at the nozzle exit with the resulting expansion wave attached to the shroud and the generated compression wave system traveling downstream (Figure 15). The pressures decreased in magnitude from P5 to P3 consistent with the underexpanded nozzle exit conditions exhausting into the shroud. The larger effective area ratio requires lower shroud pressures and this agrees with the results. Base pressure decreased near the shroud since the Mach number increases as the flow travels towards the shroud wall after going through an expansion. The flow remained attached to the shroud walls until the nozzle inlet to ambient pressure ratio equaled 53. P3 (Figure 16) showed clear evidence of detachment while P4 and P5 (Figures 17 and 18), both higher pressures initially than P3, showed little or no change throughout the test run. Some phenomenon, not measured in this investigation, occurring between the P3 and P4 of Block 1, produced a large pressure differential between these measurement stations. This differential, approximately 2.5



A. T=0 SECS



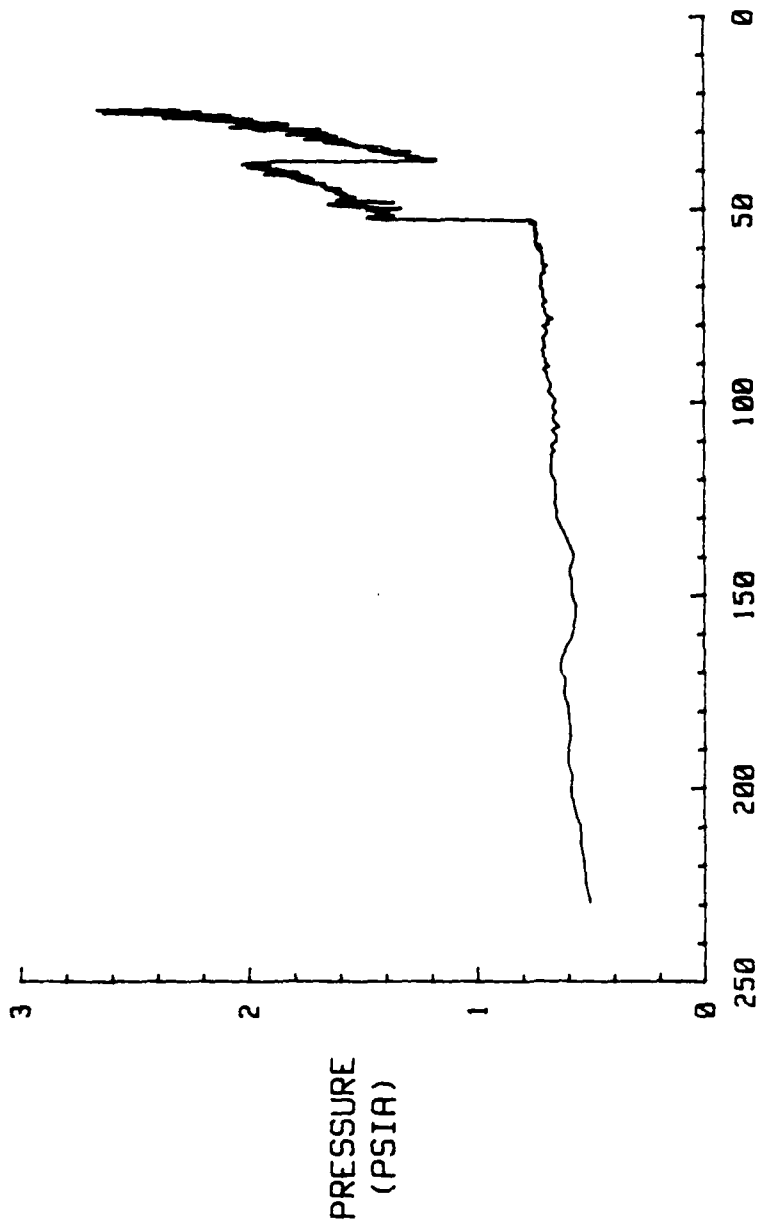
B. T=10 SECS



C. T=13 SECS

FIGURE 15. SCHLIEREN SERIES FOR CONFIGURATION 1A

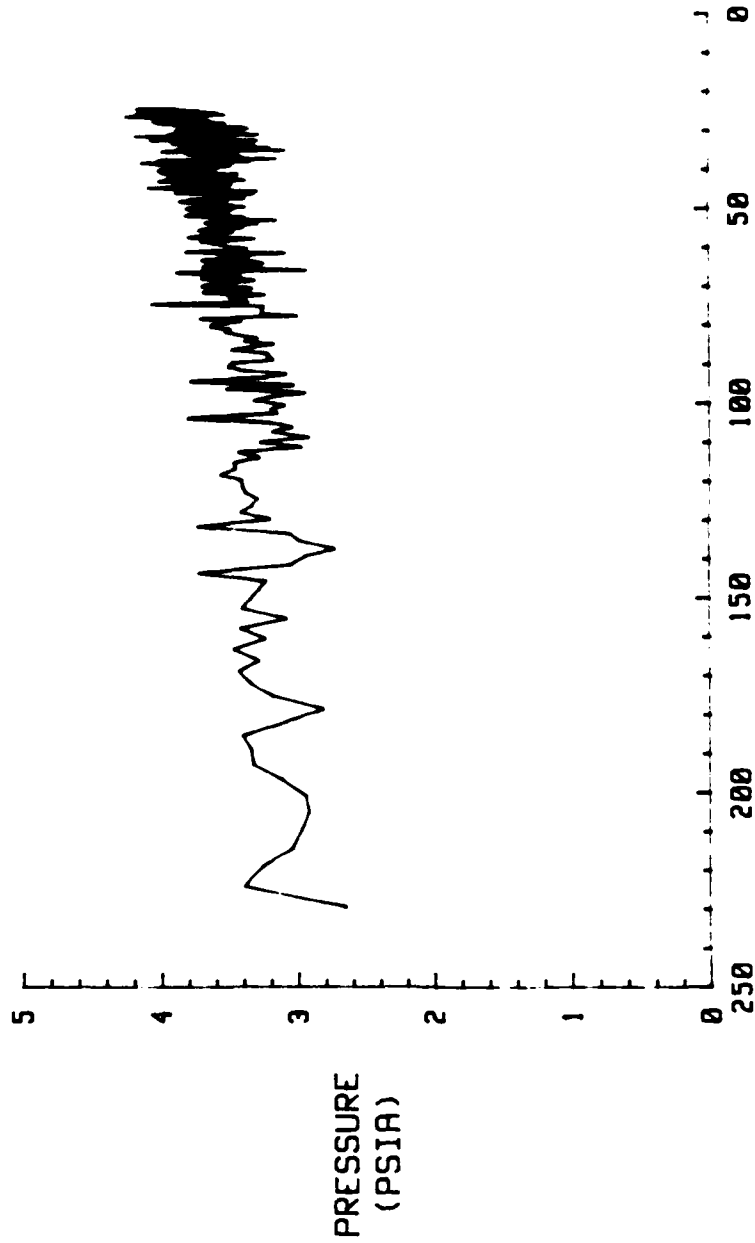
CONFIGURATION 1A



PRESSURE RATIO (PR)

FIGURE 16. P3 VS PR (CON1A)

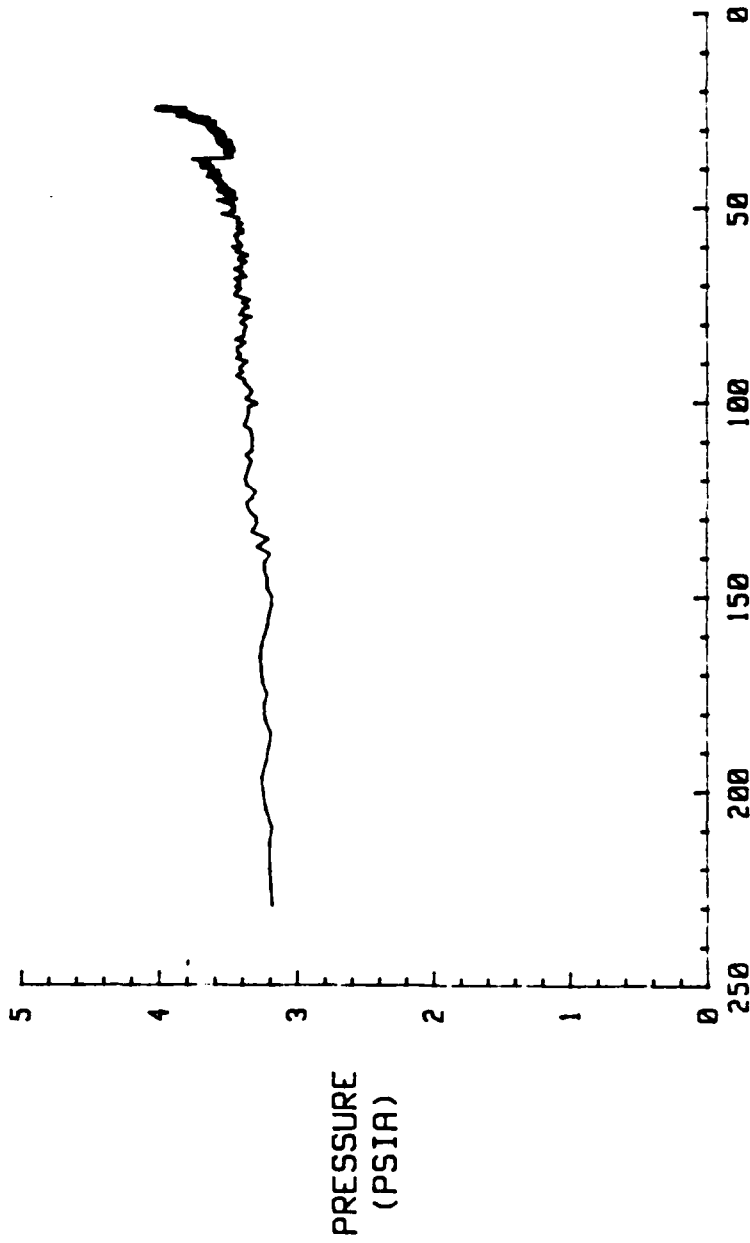
CONFIGURATION 1A



PRESSURE RATIO (PR)

FIGURE 17. P4 VS PR (CON1A)

CONFIGURATION 1A



PRESSURE RATIO (PR)

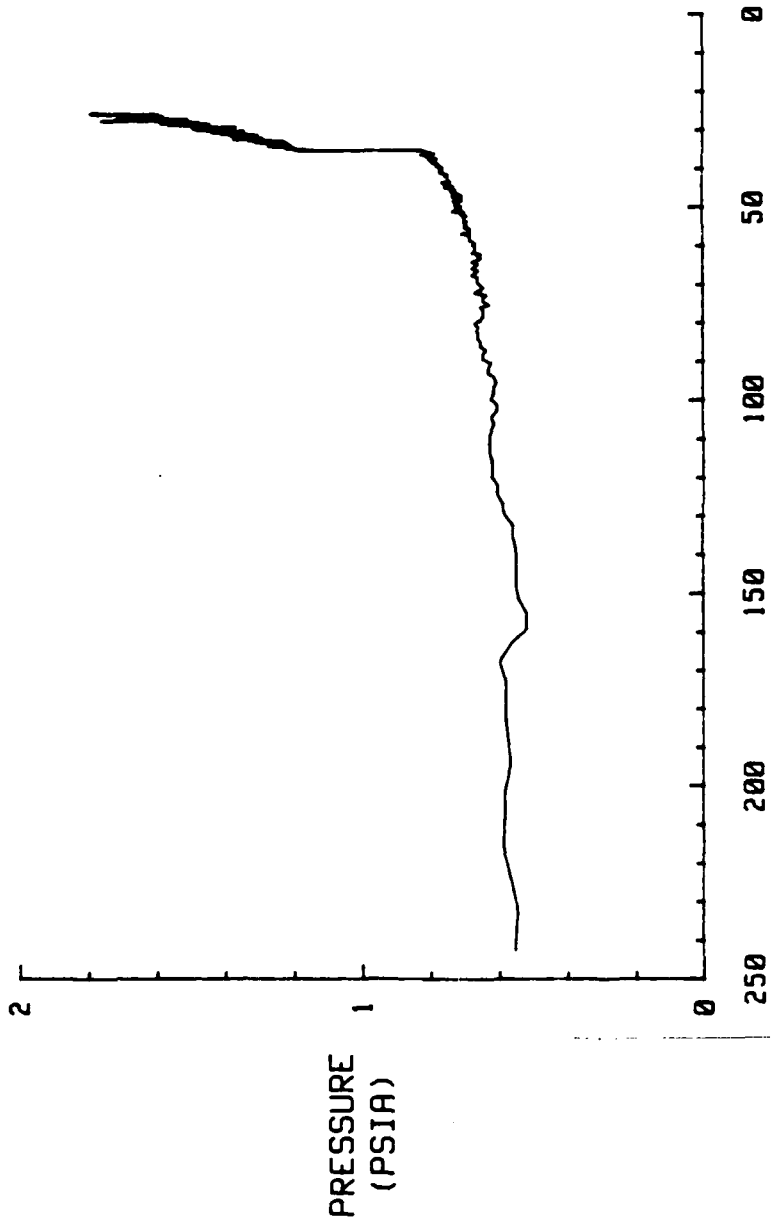
FIGURE 18. P5 VS PR (CON1A)

PRESSURE  
(PSIA)

psia, was found in both the long and short shrouded configurations. The reason for this is unclear and future researchers in this area may want to concentrate their efforts here. A pictorial history of ConlA from startup to flow detachment can be seen in Figure 15. ConlB has the same base pressures at flow start (Figure 19) and the same generated wave patterns (Figure A-1) as ConlA. However, the pressure ratio at flow detachment is 35 as compared to 53 for ConlA (Figures 16 and 19). This lower pressure ratio can be attributed to the compression wave system occurring within the longer shrouded flow channel. The longer shroud of ConlB provided the wave system with more opportunity to affect the exhaust fluid. The pressure at the shroud exit is therefore higher and more resistant to the effects of ambient pressure changes. Although separation occurred at a lower pressure ratio for ConlB, some effect of the ambient pressure change can be seen at a pressure ratio equal to 53, the separation point for ConlA. P3, of ConlB, shows a definite pressure increase until separation takes place (Figure 19). This could be the result of higher ambient back pressure leaking into the isolated base areas through the turbulent regions near the shroud (Figure A-1).

The Block 1 Schlieren photographs (Figure 15 and A-1) showed an unexpected result. A set of compression waves is shown emanating from both nozzle walls near the nozzle exit. These waves can be clearly seen on the left side middle of the photograph near the nozzle exit plane. They result from

CONFIGURATION 1B



PRESSURE RATIO (PR)

FIGURE 19. P3 VS PR (CONIB)

PRESSURE  
(PSIA)

an error made in the nozzle fabrication which caused the divergent section wall contour to be incorrect.

The Block 2 test run results were different from those of Block 1 because the pressure ratio at flow separation was the same for both the long and short shroud configurations. Even with the long shroud, the Con2B flow separated at a pressure ratio of 22 (Figures A-8 to A-11) which was the same pressure ratio for Con2A (Figures A-3 to A-6). Holmes and Matz (6) found there is some critical shroud length such that any shroud longer than this length will have a detachment pressure ratio equal to that of a system with a critical length shroud (6:5-6). There was also a well developed compression wave system in the Block 2 test runs (Figure 20) caused by the interaction of the triple nozzle flows with each other and the shroud. Since Block 1 did not have this extensive system acting on the exhaust flow exit pressure, it was more susceptible to ambient back pressure changes.

Nozzle Block 3, with an exit to throat area ratio of 4:1, showed similar flow characteristics to those of Block 1. The short shrouded configuration, Con3A, had a higher detachment pressure ratio of 70 (Figure 21), while Con3B, with the long shroud, detached at a pressure ratio of 39. The long shroud not only delayed the separation but also reduced the severity of the pressure change. As the pressure ratio approached the Con3B separation value of 39, the measured pressure began a steady increase going from 0.30 to 1.05 psia (Figure 22). Note that this pressure rise began



A. CON2A

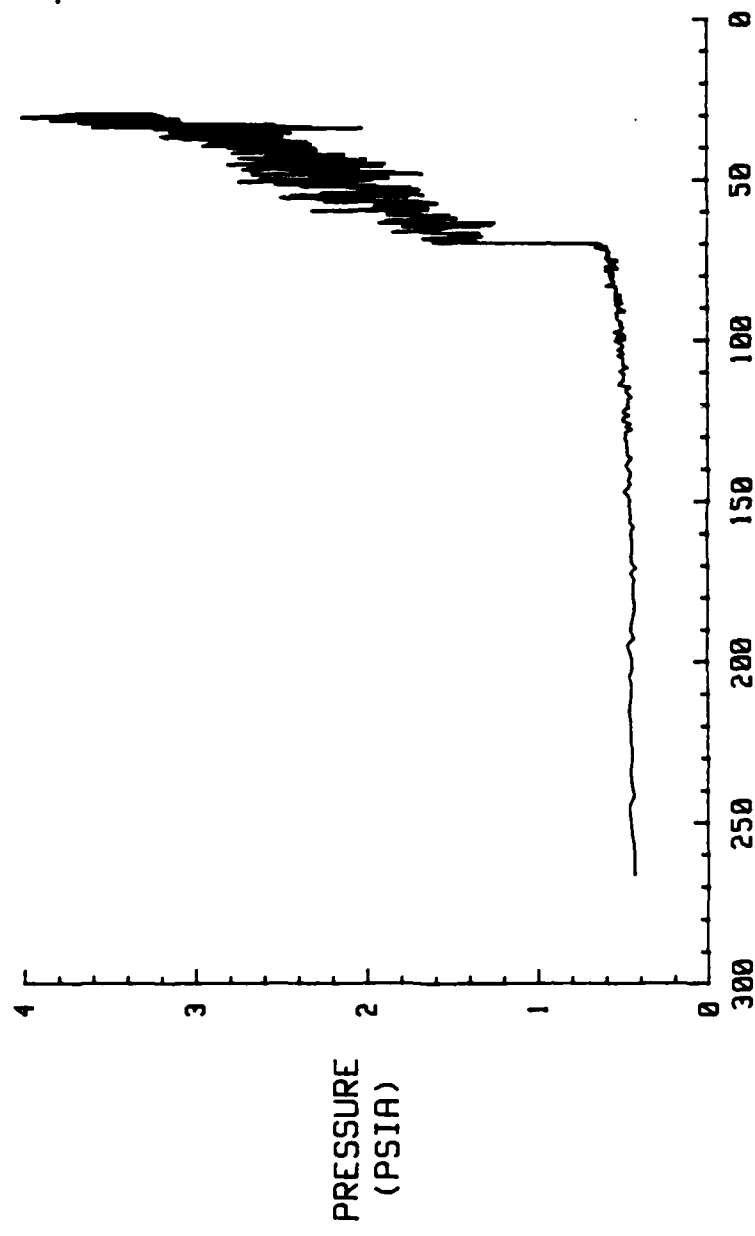


B. CON2B

FIGURE 20. SCHLIEREN SERIES FOR NOZZLE BLOCK 2

8 1 000 2 000 3 000 4 000 5 000 6 000 7 000 8 000 9 000 10 000 11 000 12 000 13 000 14 000 15 000 16 000 17 000 18 000 19 000 20 000 21 000 22 000 23 000 24 000 25 000 26 000 27 000 28 000 29 000 30 000 31 000 32 000 33 000 34 000 35 000 36 000 37 000 38 000 39 000 40 000 41 000 42 000 43 000 44 000 45 000 46 000 47 000 48 000 49 000 50 000 51 000 52 000 53 000 54 000 55 000 56 000 57 000 58 000 59 000 60 000 61 000 62 000 63 000 64 000 65 000 66 000 67 000 68 000 69 000 70 000 71 000 72 000 73 000 74 000 75 000 76 000 77 000 78 000 79 000 80 000 81 000 82 000 83 000 84 000 85 000 86 000 87 000 88 000 89 000 90 000 91 000 92 000 93 000 94 000 95 000 96 000 97 000 98 000 99 000 100 000

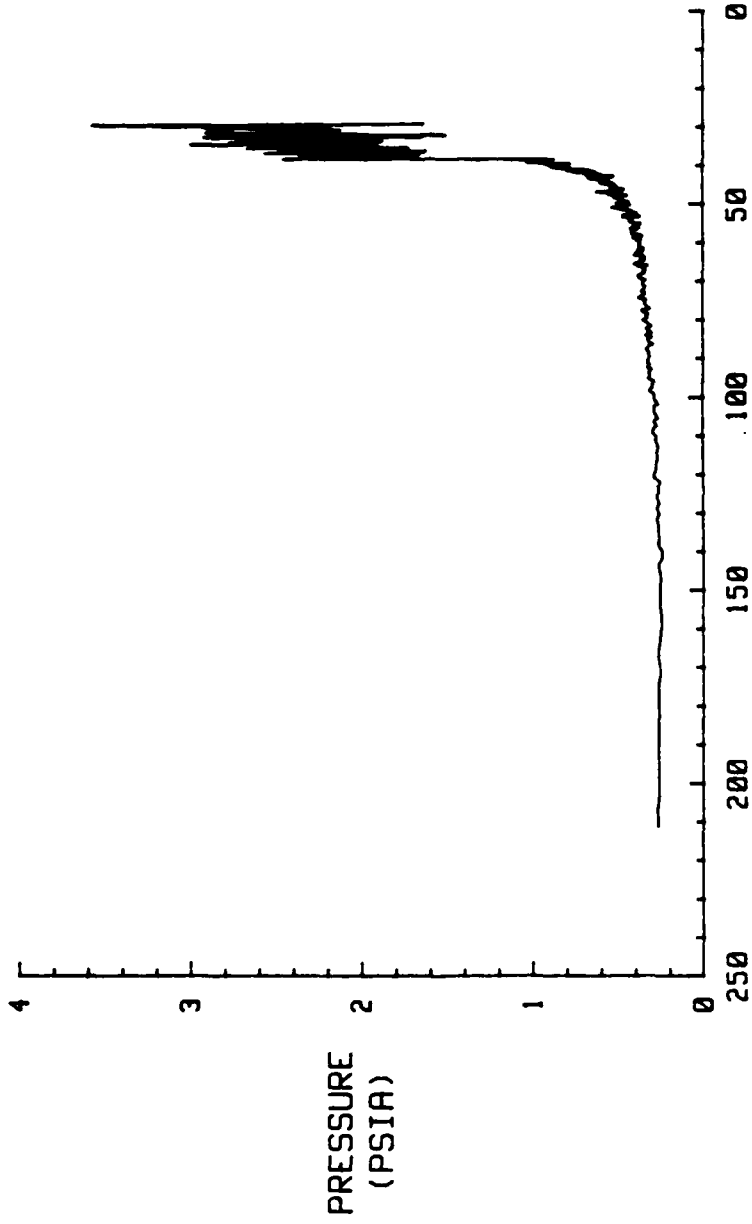
CONFIGURATION 3A



PRESSURE RATIO (PR)

FIGURE 21. P3 VS PR (CON3A)

CONFIGURATION 3B



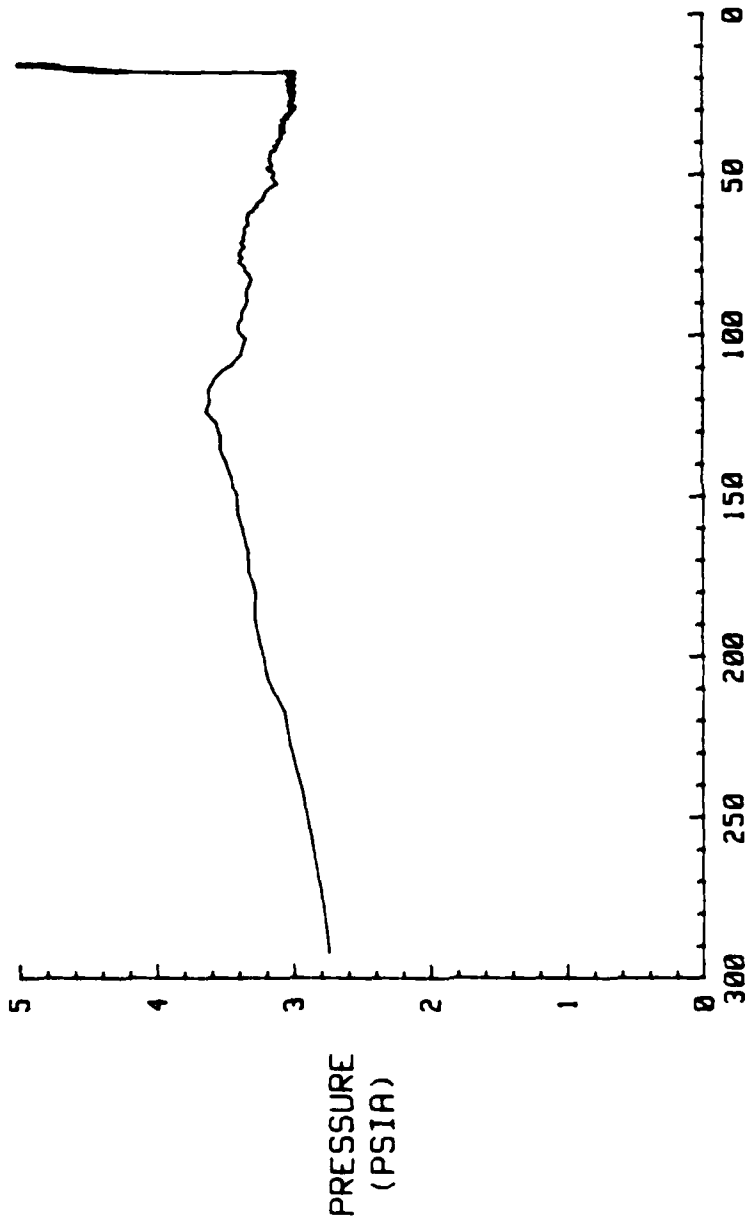
PRESSURE RATIO (PR)

FIGURE 22. P3 VS PR (CON3B)

at the same separation pressure ratio as occurred for the short shroud, Con3A, as was the case for Nozzle Block 1. The AR=4:1 for Block 3 did produce some changes in the magnitude of the base pressures. Initial values of P3 for Con1A and 1B were 0.5 and 0.58 psia respectively (Figures 16 and 19) while those of Con3A and 3B were 0.4 and 0.25 psia (Figures 21 and 22). This nozzle was used by Moran (8) and the results from this investigation were similar to those found in his experimental thesis.

For the three-dimensional nozzle block, Block 4, the exit to throat area ratio was 3:1. Initial base pressures were equal for both Con4A and Con4B. The separation pressure ratio was 18 for Con4A and 10 for Con4B, much lower than that found in the two-dimensional models, in keeping with the result that a longer shroud will delay the flow separation because of the compression wave network. This occurs since the compression system increases the pressure of the exhaust flow such that the shroud assembly exit pressure is greater than ambient pressure. There was, however, a distinct difference in the behavior of the base pressure from that of the two-dimensional configurations during the test runs. As the nozzle inlet to ambient back pressure ratio decreased, the Block 4 base pressures initially increased to a peak value of approximately 3.6 psia (Figures 23 and 24) at a pressure ratio of 122 for Con4A and 172 for Con4B and then started a gradual decrease until reaching the separation pressure ratio. This pattern of increasing and then

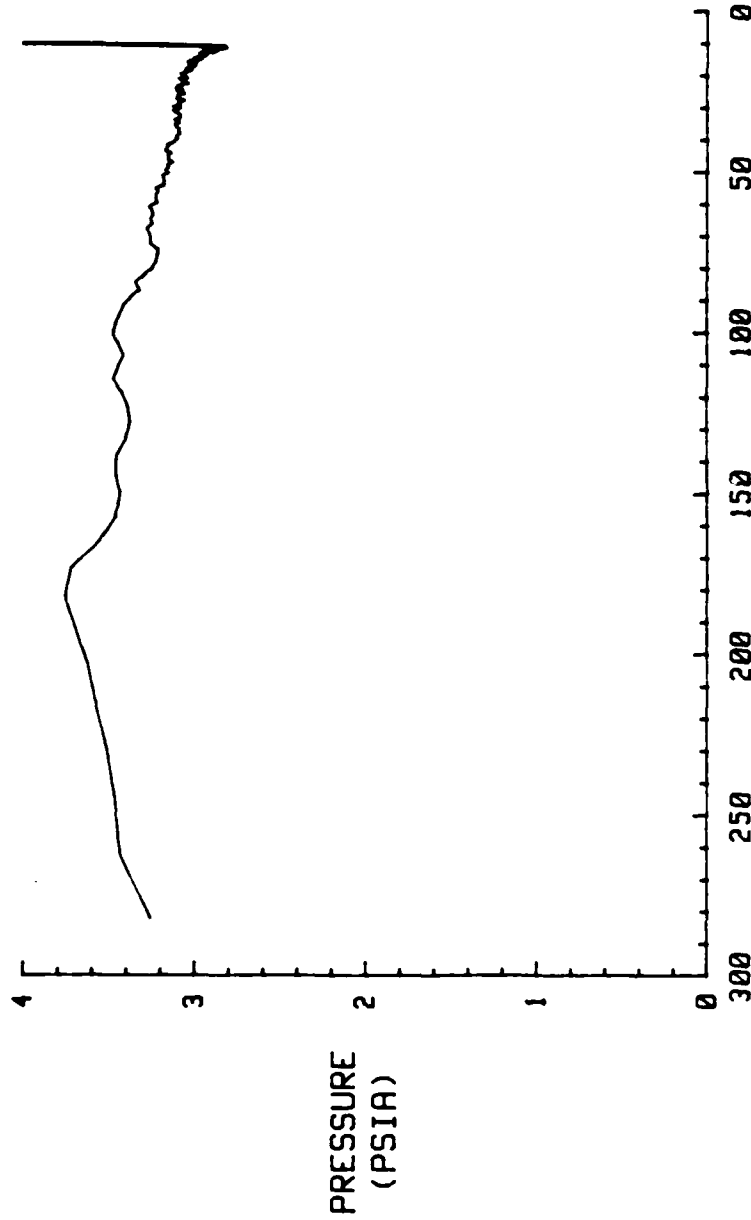
CONFIGURATION 4A



PRESSURE RATIO (PR)  
FIGURE 23. P4 VS PR (CON4A)

1 2 3 4 5 6 7 8 9 10 11 12 13 14 15 16 17 18 19 20 21 22 23 24 25 26 27 28 29 30 31 32 33 34 35 36 37 38 39 40 41 42 43 44 45 46 47 48 49 50

CONFIGURATION 4B



PRESSURE RATIO (PR)

FIGURE 24. P4 VS PR (CON4B)

PRESSURE  
(PSIA)

50

decreasing pressure could possibly be attributed to pressure leakage upstream through the boundary layer. As the pressure ratio dropped, the leakage increased until the peak pressure value was reached. It then appeared that the continued decrease of the pressure ratio reduced the leakage causing the pressure to drop. Just prior to reaching the detachment pressure ratio, Con4B showed a sharp decrease in the base pressure. This phenomenon was not noted on Con4A and no explanation for this behavior was available. Further study in this area may produce a reason for this result. A series of Schlieren photographs showing flow characteristics representative of both shroud lengths can be seen in Figure 25.

#### Shroud Pressures

This investigation showed that the shroud wall pressures behaved like those of the base pressures. The shroud data from Con1A demonstrated a similar trend to that of the base pressure in terms of a separation pressure ratio. Pressure ratio equaled 53 for separation at P9 (Figure 26), which is the shroud transducer closest to the nozzle block exit plane. The detachment pressure ratio for P3, the closest block transducer to the shroud, was also 53. As P9 was located adjacent to P3, the equal value of the separation pressure ratio was expected. This can be seen by comparing Figures 16 and 26. Con1B had the same base pressures at startup as Con1A



A. T=0 SECS



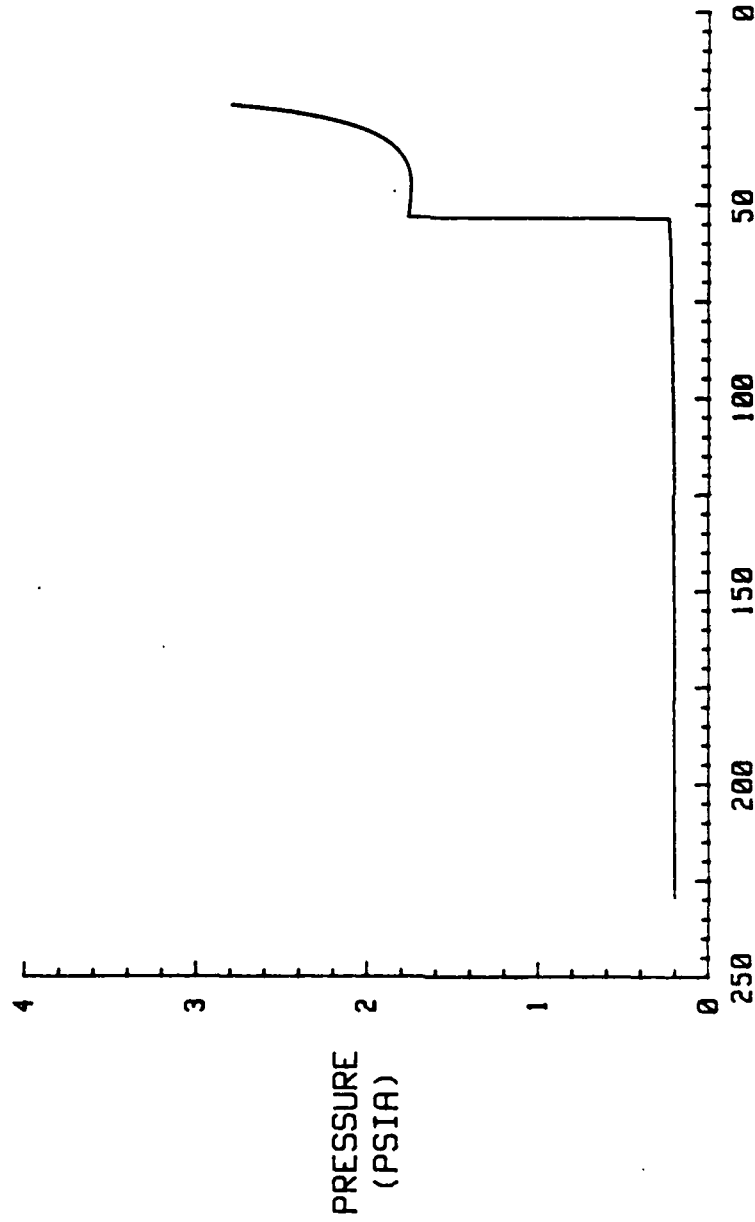
B. T=17 SECS



C. T=21 SECS

FIGURE 25. SCHLIEREN SERIES FOR NOZZLE BLOCK 4

CONFIGURATION 1A



PRESSURE RATIO (PR)

FIGURE. 26. P9 VS PR (CONIA)

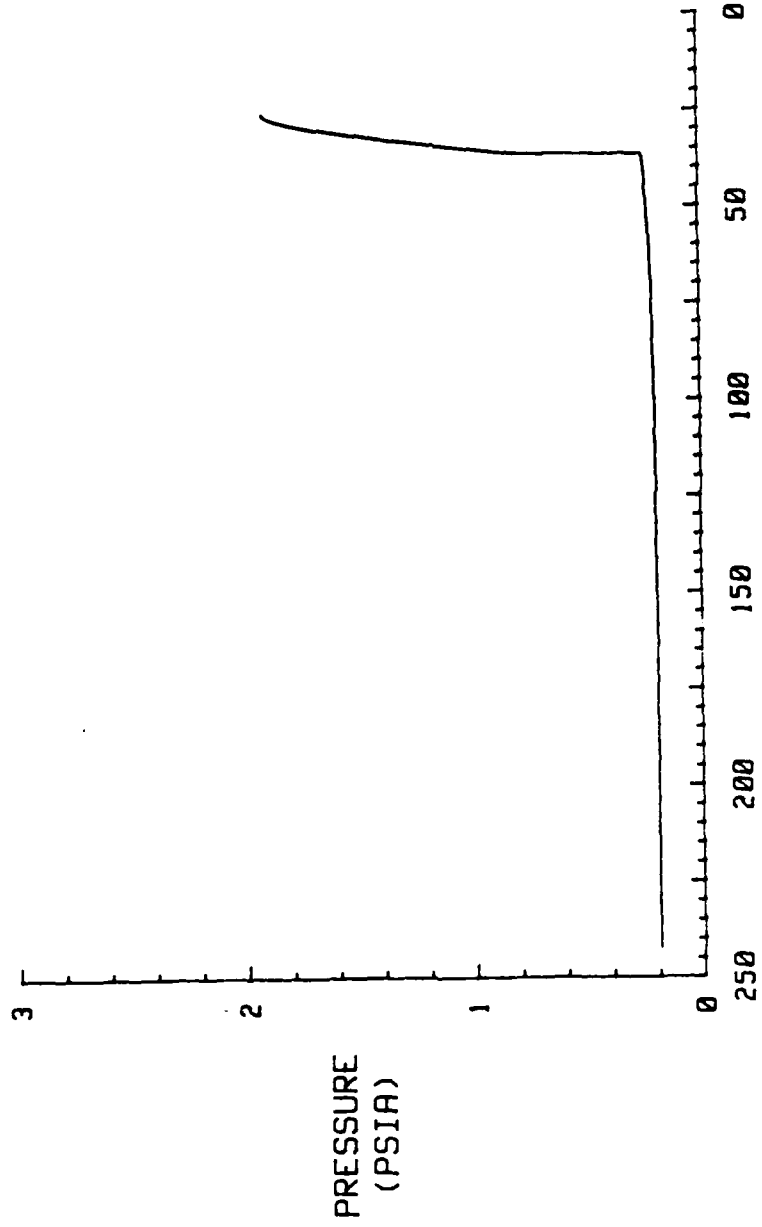
with a lower detachment pressure ratio of 36 (Figure 27). The longer shroud length contributed to the reduced pressure ratio just as occurred in the base pressure results. Shroud flow separation took place at increasing pressure ratio the farther from the nozzle exit plane the measurement station was located. At the farthest station for Con1B, P14, the flow was unable to attach with the pressure ratio equal to 240, while pressure ratio equaled 36 at station P9, the closest station to the nozzle exit plane.

The shroud pressures for the second nozzle block exhibited similar trends. For both Con2B and Con2A the flow separation pressure ratio was the same for the identically positioned transducers P7, P8, and P9 (Figures B-2 to B-4 and B-6 to B-8). Equal separation pressure ratios also occurred in the pressure transducers, P3, P4, and P5 (Figures A-3 to A-5).

Shroud data from configurations 3A and 3B continued the trend of the nozzle assembly with the shorter shroud having the higher detachment pressure ratio. Shroud flow separation occurred at a pressure ratio of 70 for Con3A and a pressure ratio equal to 38 for Con3B for the same transducer position, P5 (Figures 28 and 29). The other identically placed shroud transducers for both Con3A and Con3B, P6 and P7, exhibited the same behavior of constant pressure rise throughout the run.

Flow detachment took place at the pressure ratio equal to 30 for Con4A. However, Con4B never experienced any

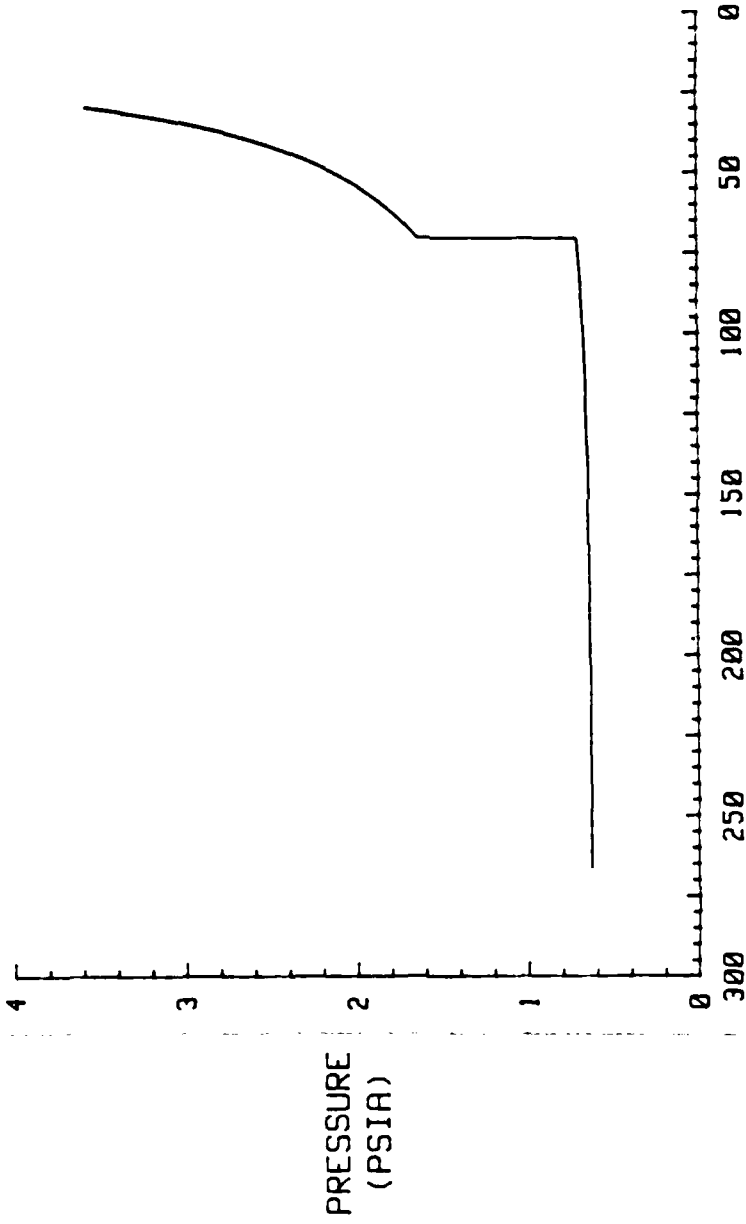
CONFIGURATION 1B



PRESSURE RATIO (PR)

FIGURE. 27. P9 VS PR (CON1B)

CONFIGURATION 3A

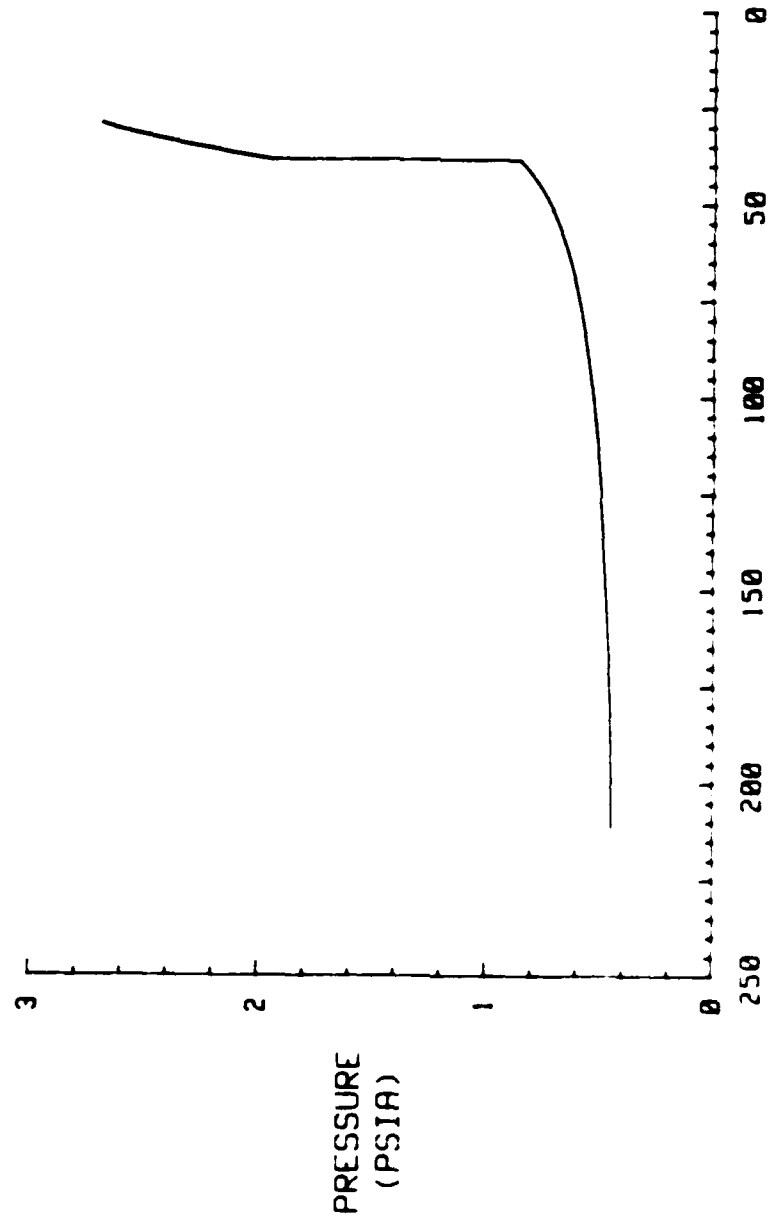


56  
PRESSURE  
(PSIA)

PRESSURE RATIO (PR)

FIGURE 28. P5 VS PR (CON3A)

CONFIGURATION 3B



PRESSURE RATIO (PR)  
FIGURE. 29. P5 VS PR (CON3B)

separation. Instead, P6, P7 and P11 all increased continuously throughout the run as can be seen in Figures B-9, B-10 and B-14. The pressure measurement stations 8, 9, and 10 (Figures B-11 through B-13) showed a decrease in the shroud pressure until the pressure ratio was approximately 30. This difference in behavior was caused by the jet exhaust interaction not completely isolating the shroud walls from ambient conditions. The exhaust gas expanded in a circular fashion such that the interactions of the four nozzle flows left gaps, adjacent to the shroud walls, along the vertical and horizontal centerlines of the nozzle exit plane. This allowed the ambient conditions to be felt by the shroud pressure measurement stations which were on the shroud centerline oriented perpendicular to the vertical centerline of the nozzle exit plane. Goethert commented on this in his work with a 4 nozzled cluster (4:12).

## VI CONCLUSIONS

Pressure and flow relationships of four nozzle blocks and two shroud lengths were studied over a range of test conditions. The apparatus and the associated instrumentation were satisfactory for the purpose of this investigation. The results lead to the following conclusions:

1. The exhausts of the nozzles interact with each other and the shroud at high nozzle inlet to ambient back pressure ratios. This interaction affects the pressures along the nozzle exit plane and the shroud walls. Whenever this interaction isolates the flow channel from the ambient back pressures, a positive increase in the pressure thrust term can be realized. The expansion also creates a larger effective nozzle exit area, thereby increasing the exit Mach number, pressure and velocity with a resultant increase in the momentum thrust term.

2. Shroud length affects the nozzle inlet to ambient pressure ratio at which the flow separates from the shrouded walls. The longer shroud permitted operation at a lower pressure ratio before flow detachment occurred. The lower pressure ratio means the positive increases in the momentum and pressure thrust terms will develop at lower altitudes as the nozzle assembly ascends. The benefits from delayed separation, such as increased exit area and velocity, can therefore be utilized for a longer period of time.

3. The three-dimensional nozzle exhaust interactions was very different from that of the two-dimensional nozzle. The three-dimensional flow interactions did not entirely isolate the shroud from the ambient conditions. The base pressures were initially isolated from ambient conditions, much like the two-dimensional model, and then experienced separation as the pressure ratio dropped. Shroud pressures, however, showed no sign of being isolated from the ambient conditions. As the back pressure increased, so did the shroud wall pressures. The only exception to this was the shroud measurement station closest to the nozzle exit plane. The initial nozzle flow expansion trapped an area of lower pressure in that region. Under operating conditions when the expansion does not isolate the shroud pressures completely, there could be a decrease in nozzle performance.

4. Nozzle performance is highly dependent upon system geometry, nozzle spacing, and shroud length. The three-dimensional nozzle assembly results showed potential for a decrease in nozzle performance. Performance increases could occur because of a change in flow gas dynamics and the effective nozzle exit area. The flow changes which improve performance are increased exit exhaust velocity, Mach number, and exit to nozzle inlet pressure ratio. These occur as a result of the effective nozzle exit area increase for a started nozzle and shroud assembly.

## VII RECOMMENDATIONS

The following recommendations are suggested for the continuation of this work with shrouded nozzles:

1. Different shroud lengths should be tested in order to determine a method of calculating a critical shroud length for the two-dimensional nozzles.

2. Make improvements to the vacuum system to allow for steady state testing at various ambient conditions.

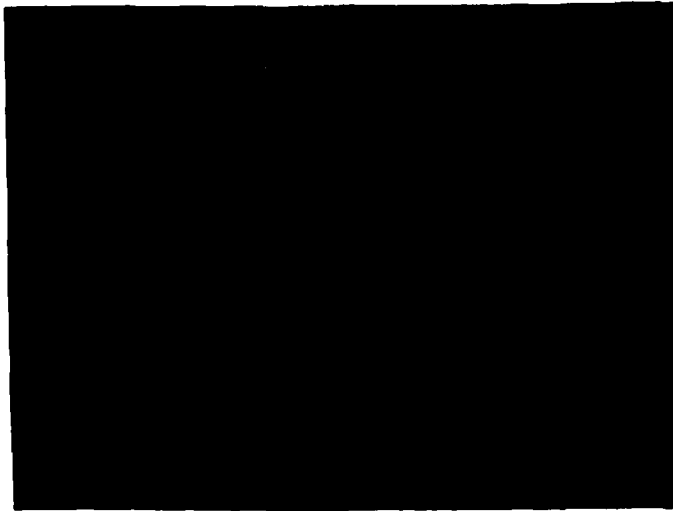
3. Obtain a high speed camera capable of filming the events occurring within the test section. Since pressure data can be taken with as little as 40 microseconds between each pressure reading, a camera with comparable capability would greatly improve data acquisition.

4. More three-dimensional models should be tested to further evaluate the effect shrouding has on the base pressure and the shroud pressure. This would improve the understanding of the real life problems which can occur in shrouded rocket nozzles.

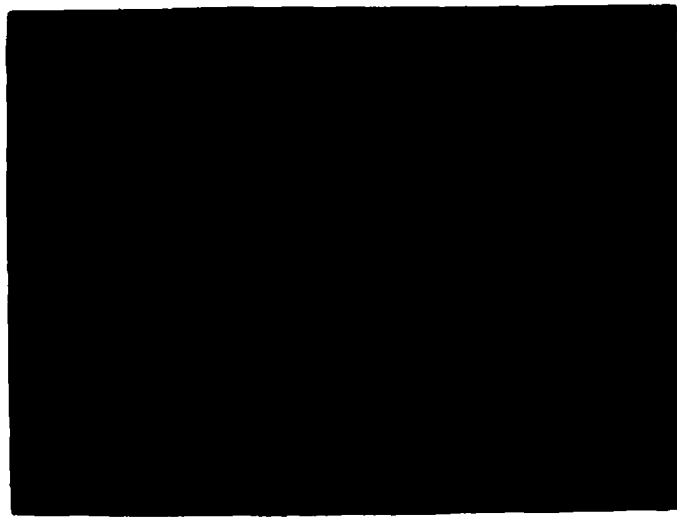
## BIBLIOGRAPHY

1. Anderson, J. D., Jr. Fundamentals of Aerodynamics. New York:McGraw-Hill Book Company, 1984.
2. Bjurstrom, D. R. An Experimental Study of Clustered, Two-Dimensional Rocket Nozzles. MS Thesis, Wright-Patterson AFB, Ohio:Air Force Institute of Technology, December 1984.
3. Daley, D. H. "A Nozzle Operating Diagram", Bulletin of Mechanical Engineering Education, 6:245-257 (April 1967).
4. Goethert, B. H. Studies of the Flow Characteristics and Performance of Multi-Nozzle Rocket Exhausts. AEDC-TR-59-16. Arnold AFS, Tennessee:ARO, Inc., October (1959) (AD 313-155).
5. Hill, P. G. and C. R. Peterson. Mechanics and Thermodynamics of Propulsion. Reading:Addison-Wesley Publishing Company, 1970.
6. Holmes, B. K. and R. J. Matz. An Investigation of the Multi-Nozzle Rocket Shroud Concept. AEDC-TR-65-249. Arnold AFS, Tennessee:ARO, Inc., February 1965 (AD 369808).
7. Hoffman, J. D. and M. J. Zucrow. Gas Dynamics, Volume I. New York:John Wiley and Sons, Inc., 1976.
8. Moran, J. R. An Experimental Study of Clustered Nozzles with Variable Shrouds. MS Thesis, Wright-Patterson AFB, Ohio:Air Force Institute of Technology, December 1985.
9. Sutton, G. P. Rocket Propulsion Elements (Fourth Edition). New York:John Wiley and Sons, 1976.

Appendix A



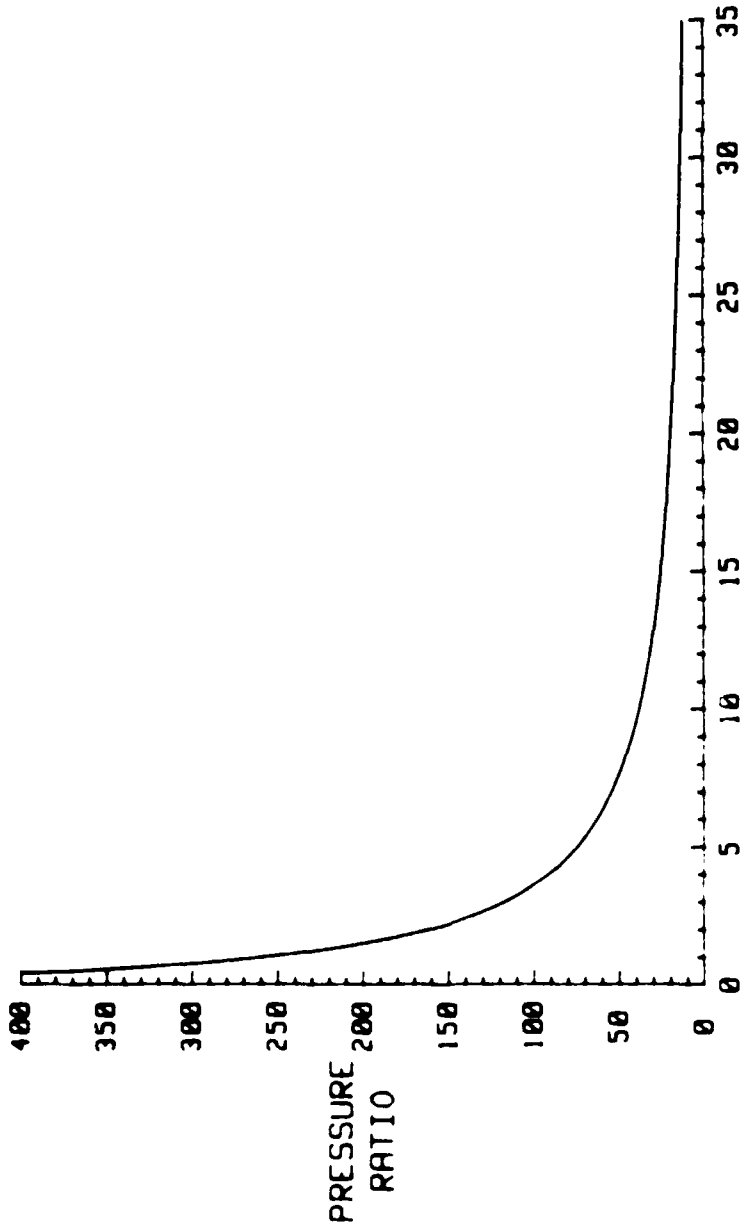
R. T-0 SECS



B. T-24 SECS

ALL INFORMATION CONTAINED HEREIN IS UNCLASSIFIED

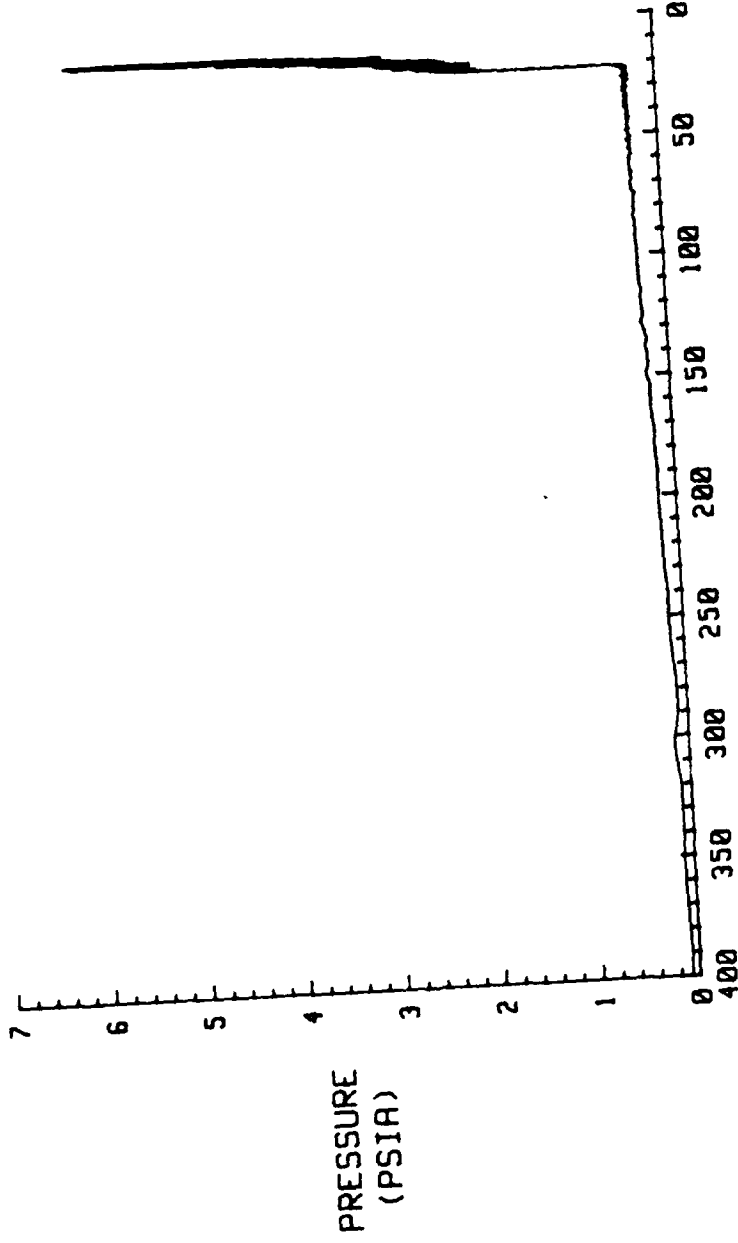
CONFIGURATION 2A



TIME (SECS)

FIGURE A-2. PR VS TIME (CON2A)

CONFIGURATION 2A

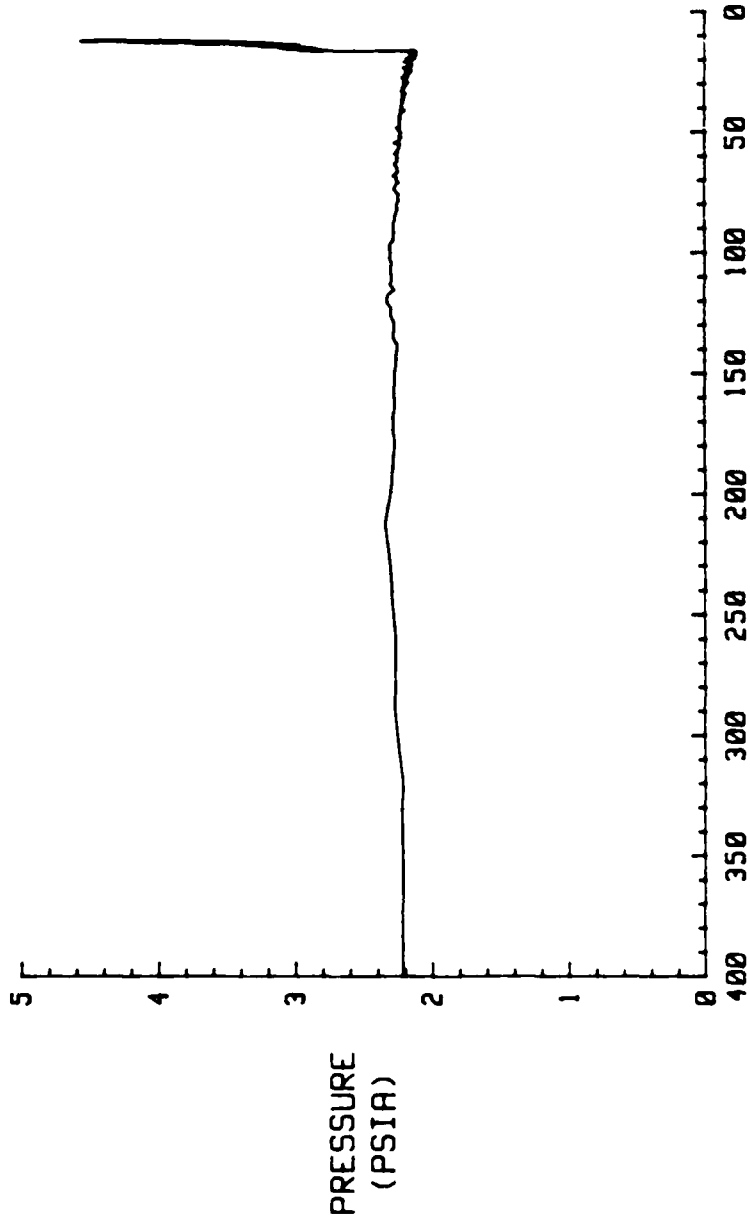


PRESSURE RATIO (PR)

FIGURE A-3. P3 VS PR (CON2A)

66

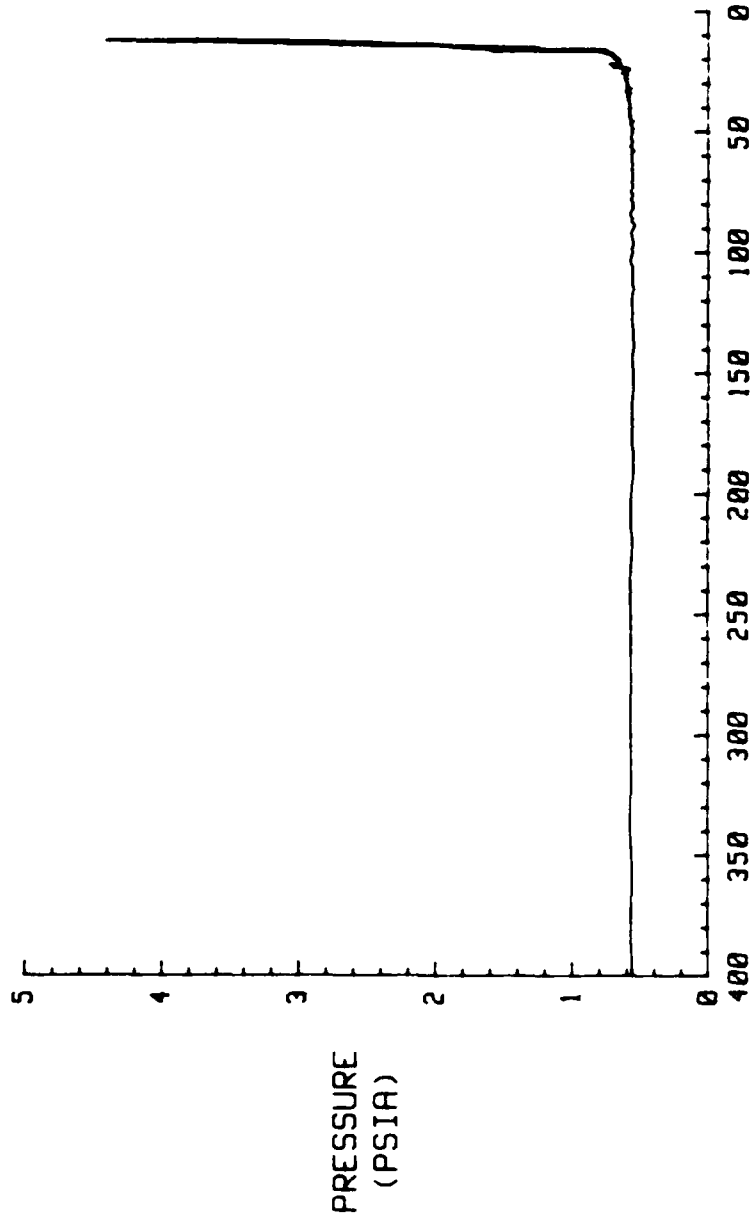
CONFIGURATION 2A



PRESSURE RATIO (PR)

FIGURE A-4. P4 VS PR (CON2A)

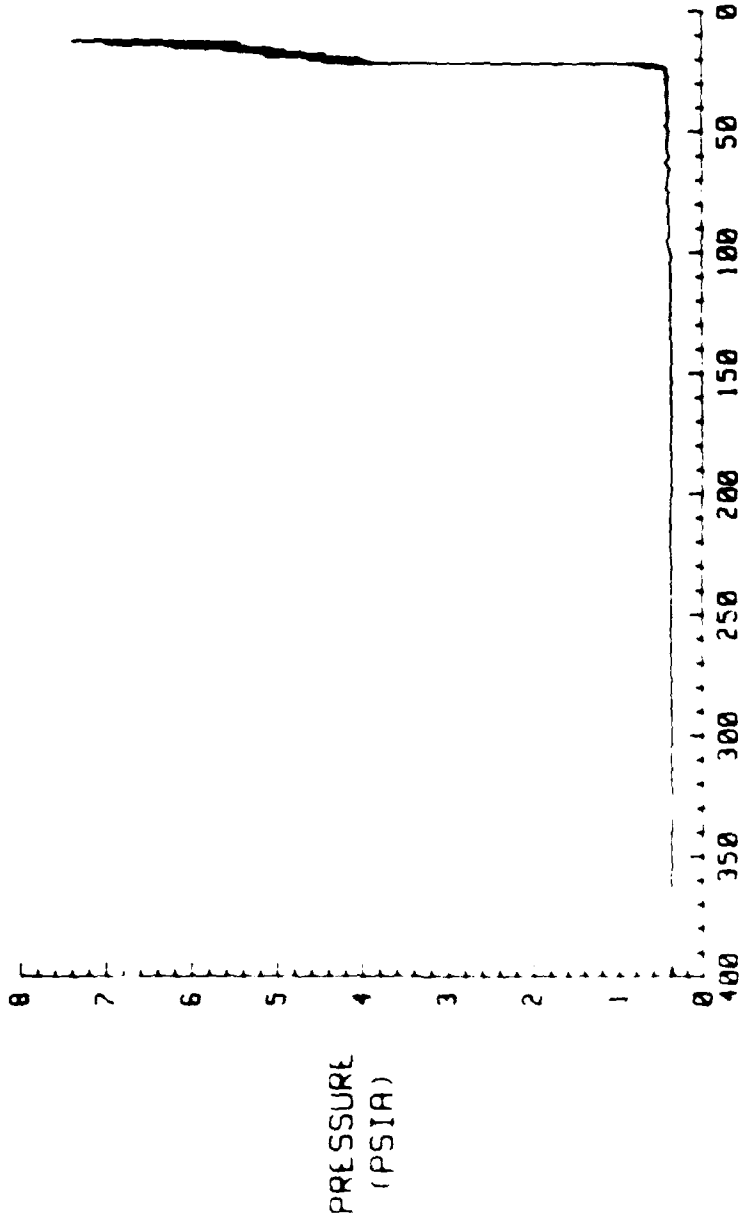
CONFIGURATION 2A



PRESSURE RATIO (PR)

FIGURE A-5. P5 VS PR (CON2A)

CONFIGURATION 2A



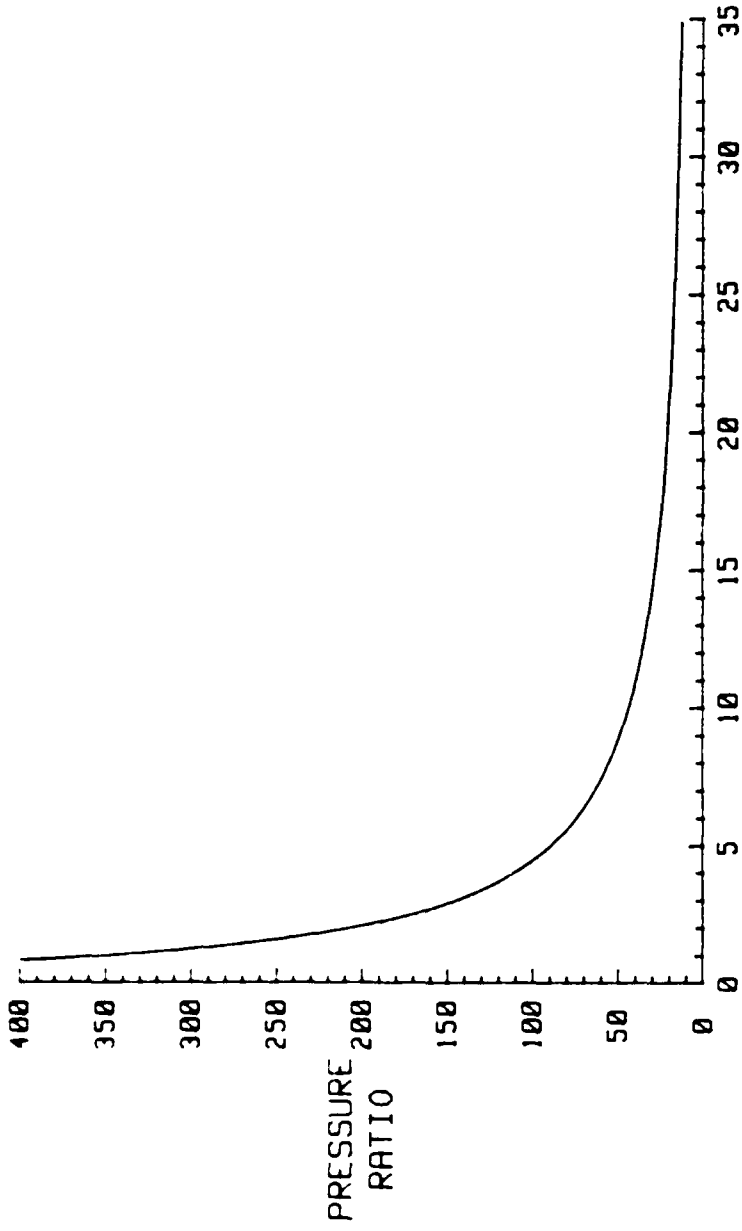
PRESSURE RATIO (PR)

FIGURE A-6. P6 VS PR (CON2A)

PRESSURE  
(PSIA)

69

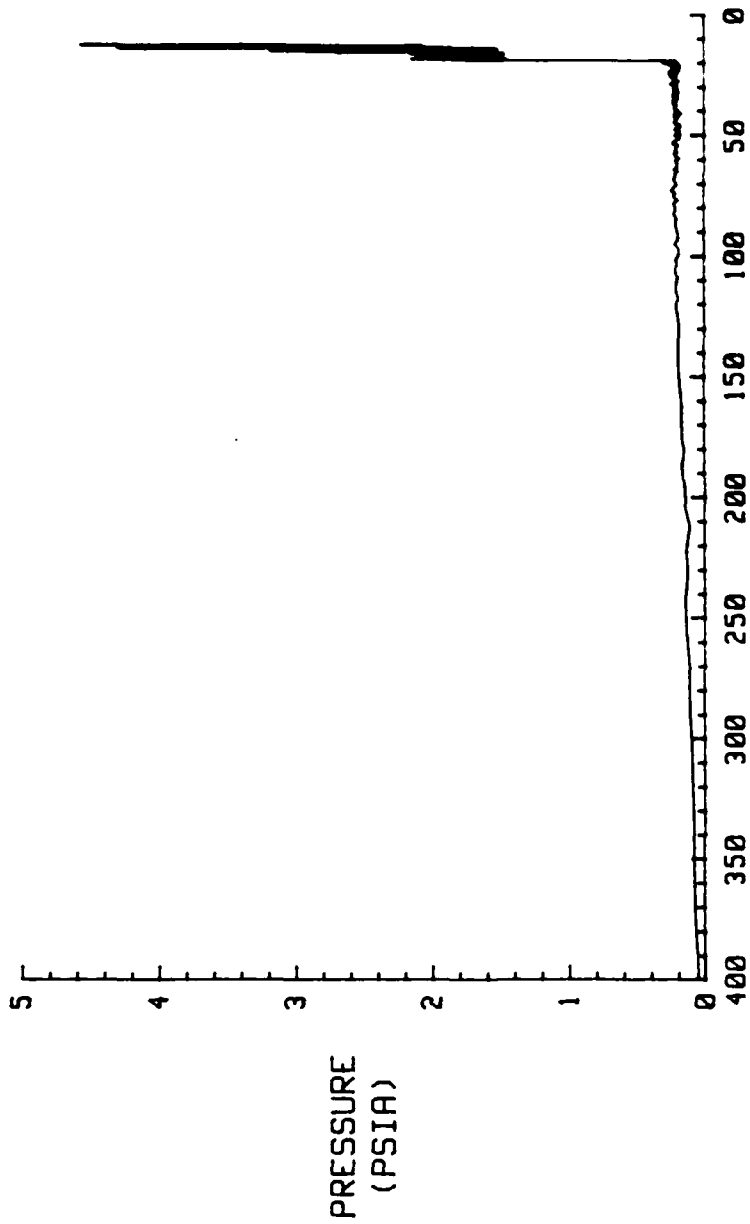
CONFIGURATION 2B



TIME (SECS)

FIGURE A-7. PR VS TIME (CON2B)

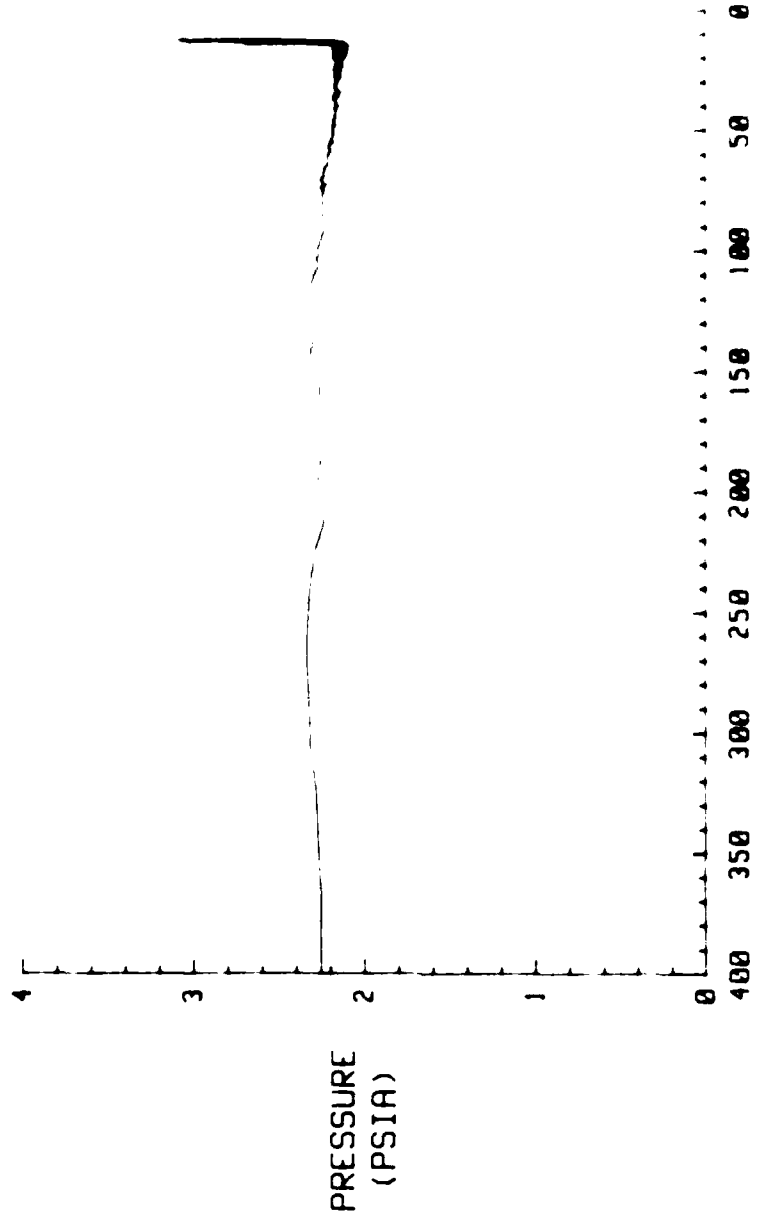
CONFIGURATION 2B



PRESSURE RATIO (PR)

FIGURE A-8. P3 VS PR (CON2B)

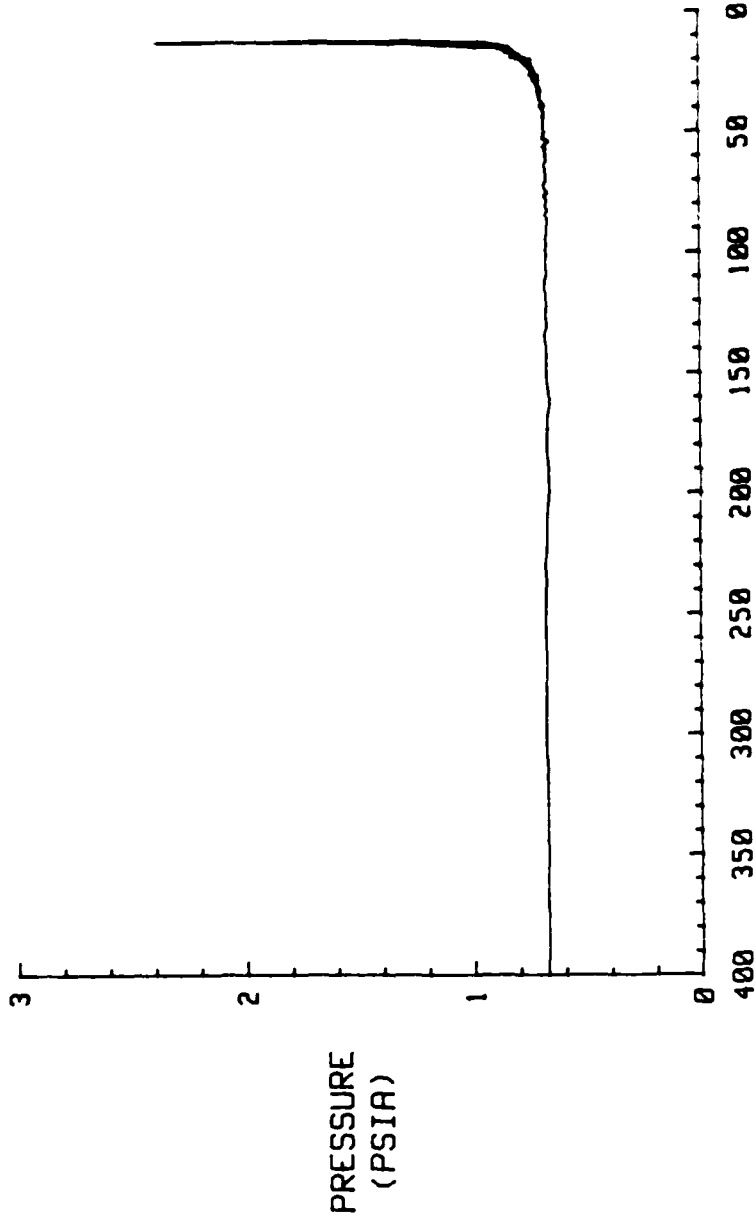
CONFIGURATION 2B



PRESSURE RATIO (PR)

FIGURE A-9. P4 VS PR (CON2B)

CONFIGURATION 2B

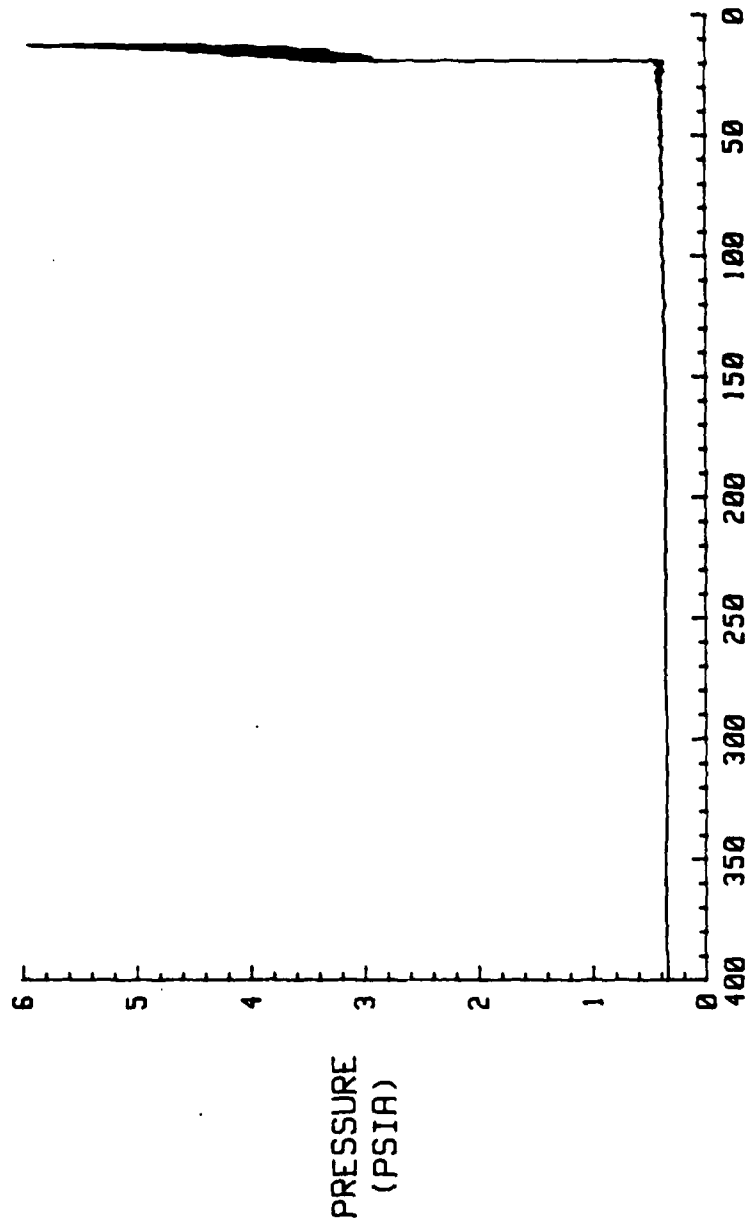


PRESSURE RATIO (PR)

FIGURE A-10. P5 VS PR (CON2B)

PRESSURE  
(PSIA)

CONFIGURATION 2B



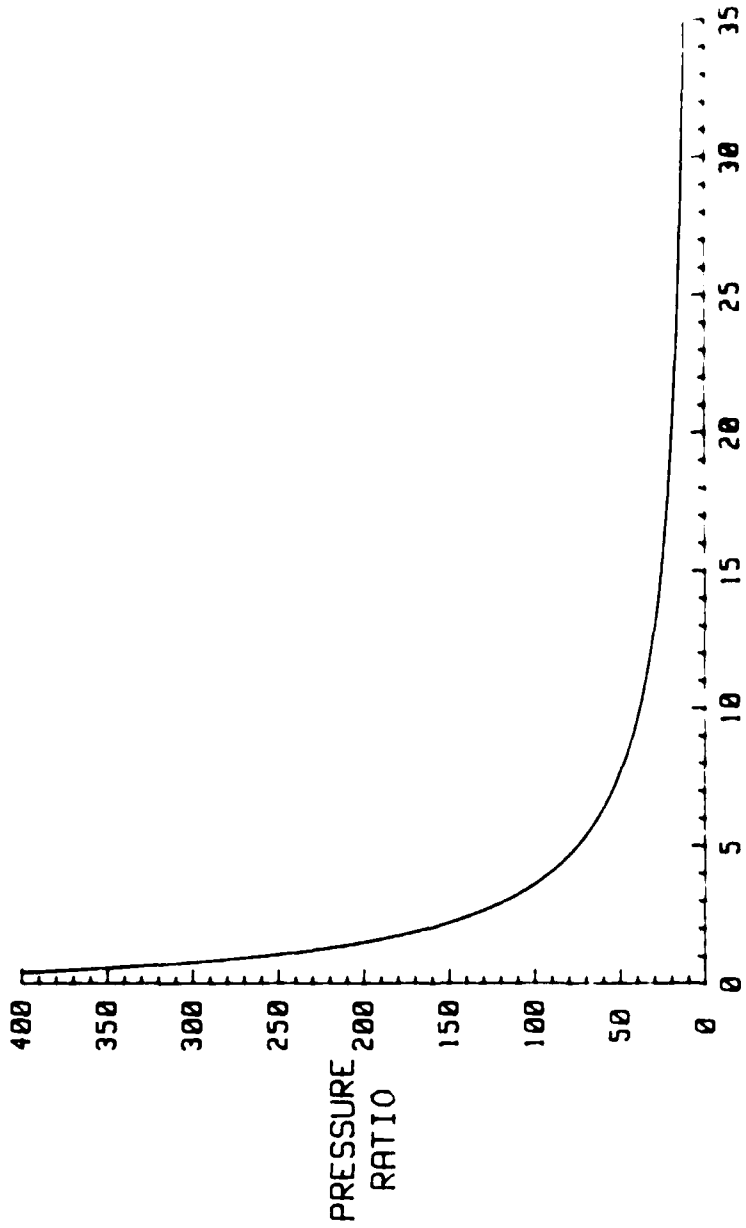
PRESSURE RATIO (PR)

FIGURE A-11. P6 VS PR (CON2B)

PRESSURE  
(PSIA)

Appendix B

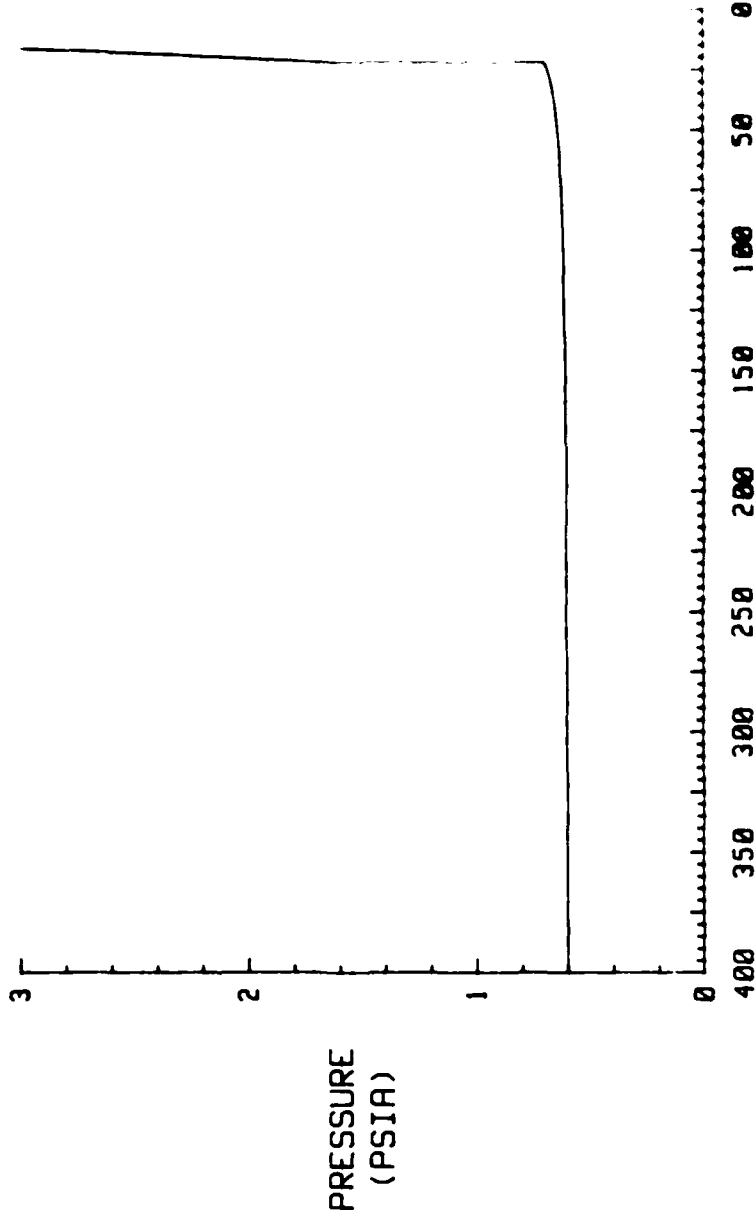
CONFIGURATION 2A



TIME (SECS)

FIGURE B-1. PR VS TIME (CON2A)

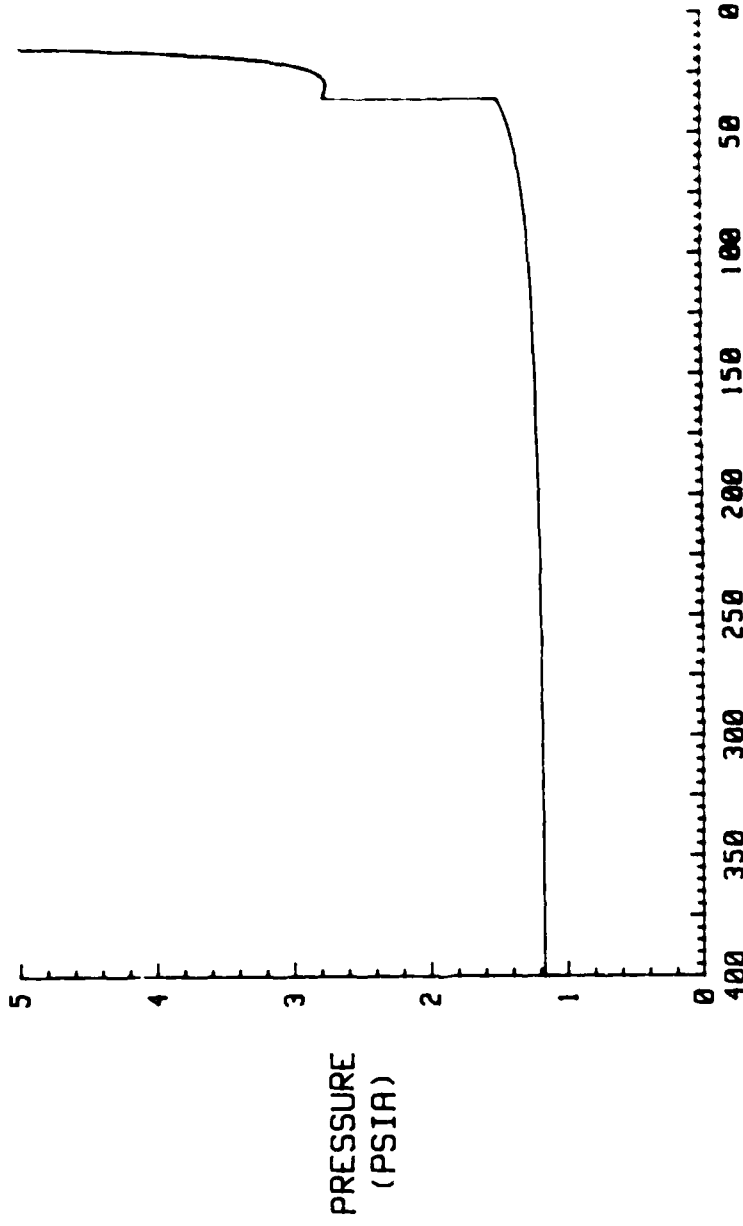
CONFIGURATION 2A



PRESSURE RATIO (PR)

FIGURE. B-2. P7 VS PR (CON2A)

CONFIGURATION 2A

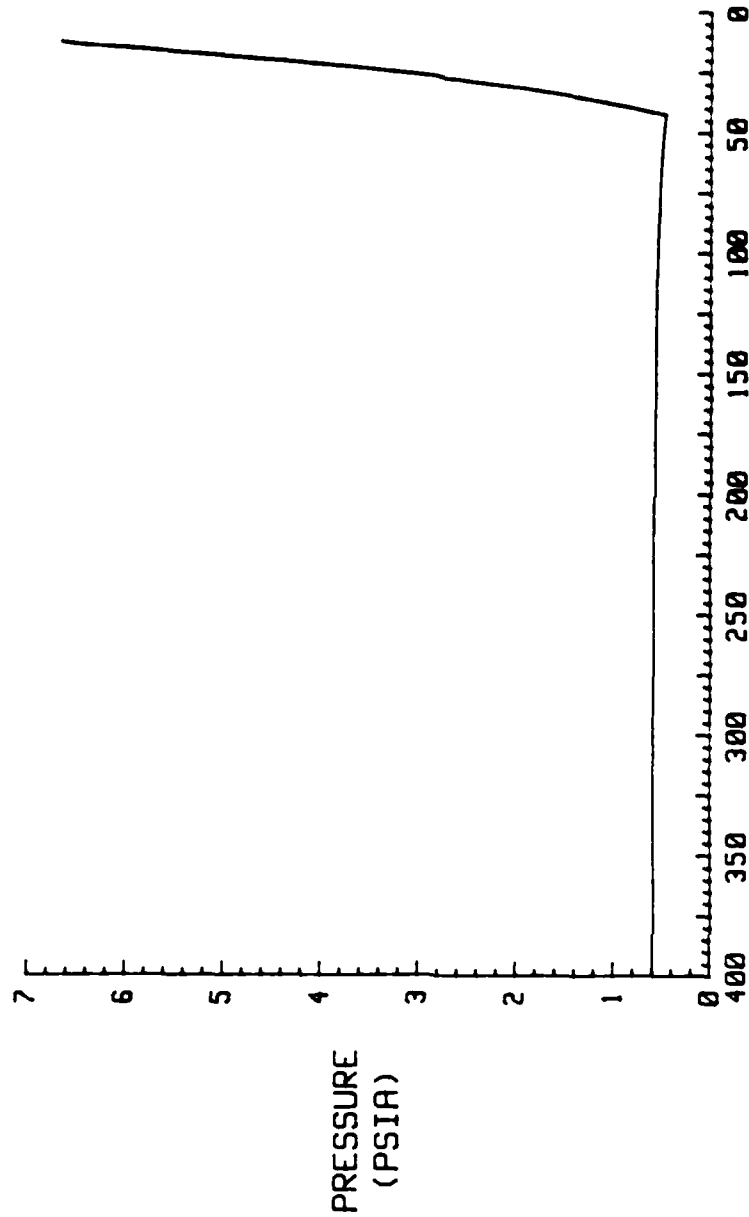


78

PRESSURE RATIO (PR)

FIGURE. B-3. P<sub>B</sub> VS PR (CON2A)

CONFIGURATION 2A



PRESSURE RATIO (PR)

FIGURE. B-4. P9 VS PR (CON2A)

PRESSURE  
(PSIA)

CONFIGURATION 2B

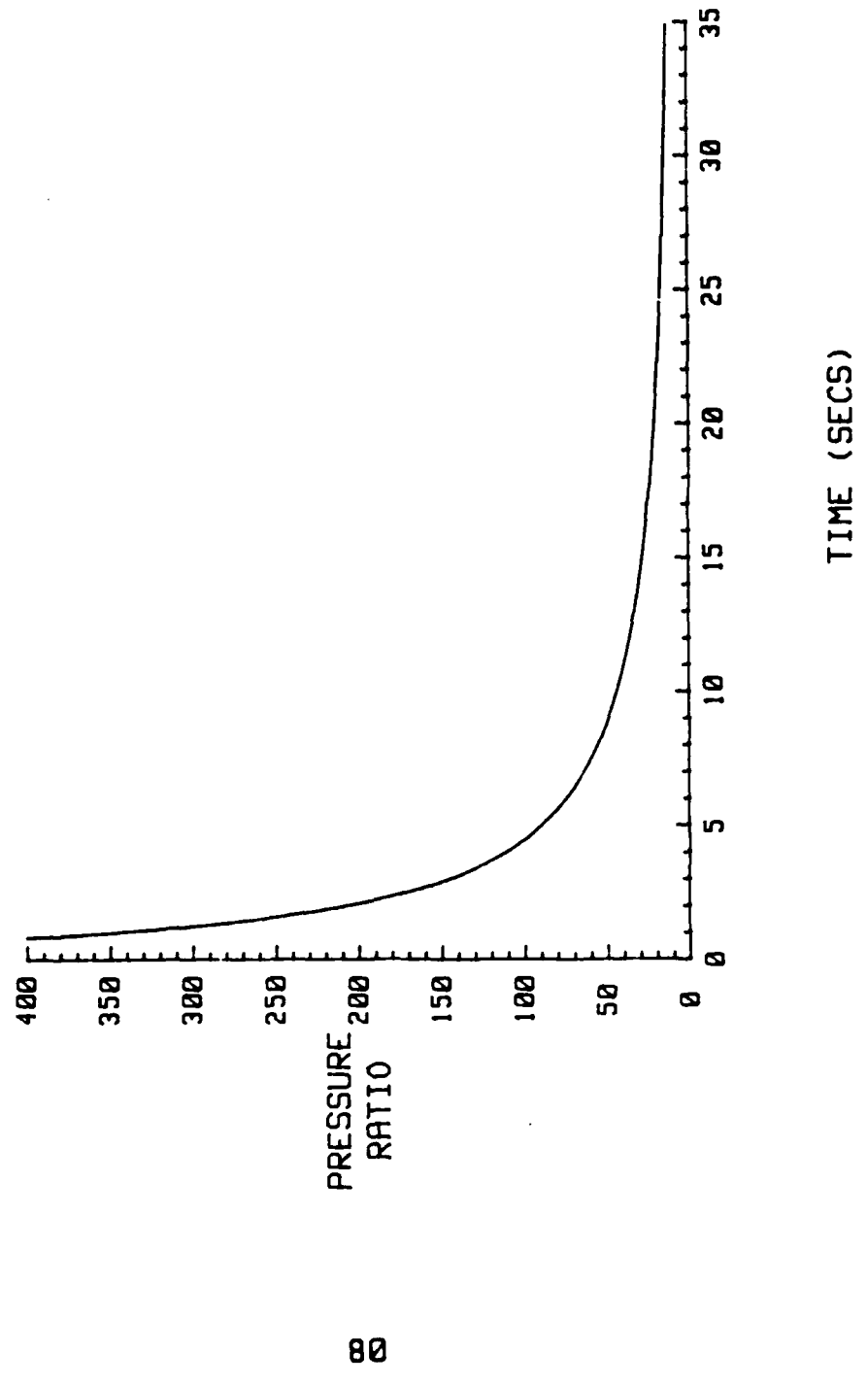
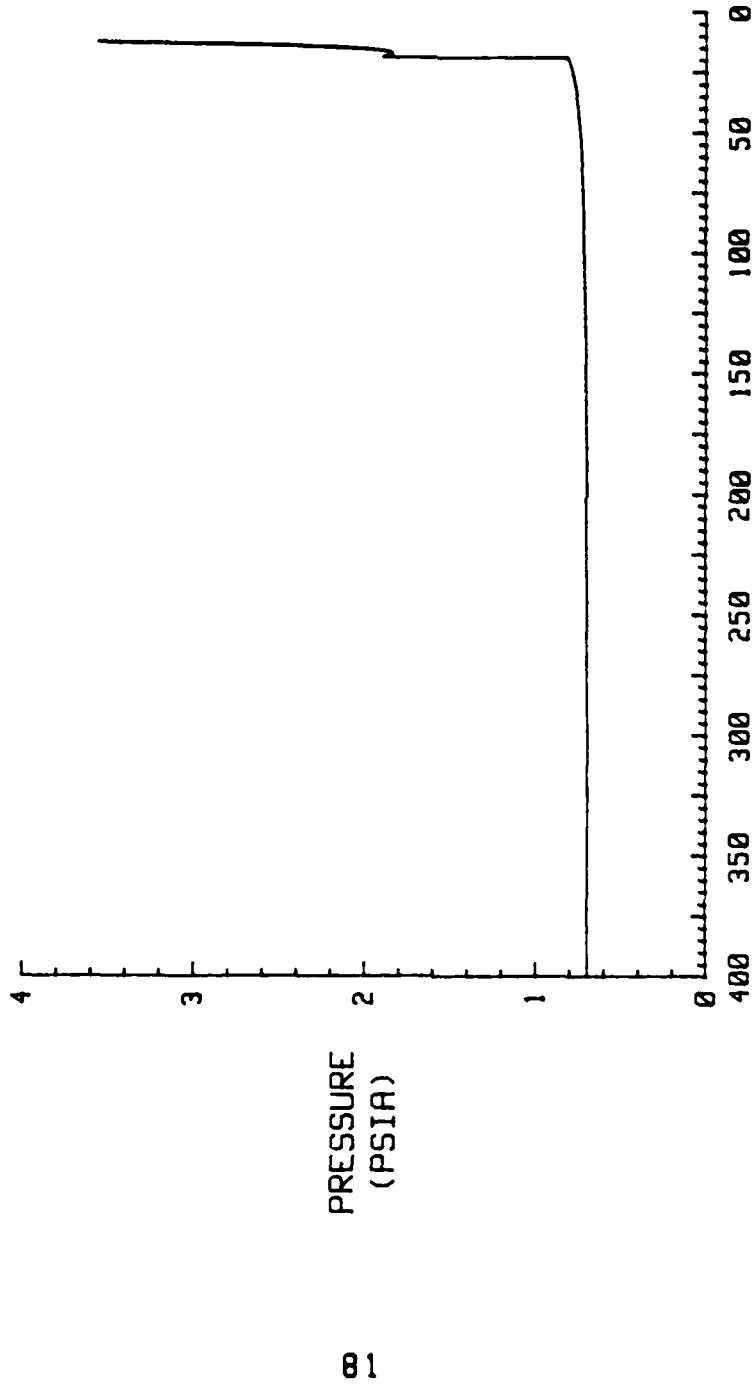


FIGURE B-5. PR VS TIME (CON2B)

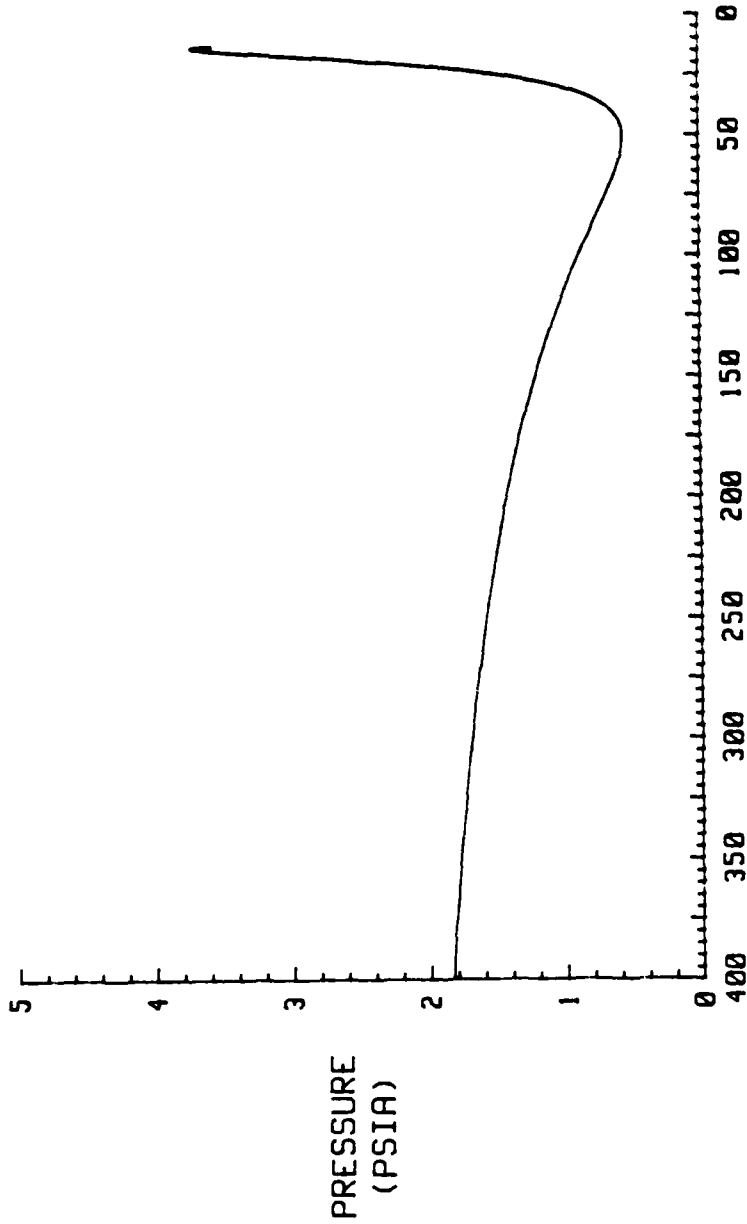
CONFIGURATION 2B



PRESSURE RATIO (PR)

FIGURE. B-6. P7 VS PR (CON2B)

CONFIGURATION 2B

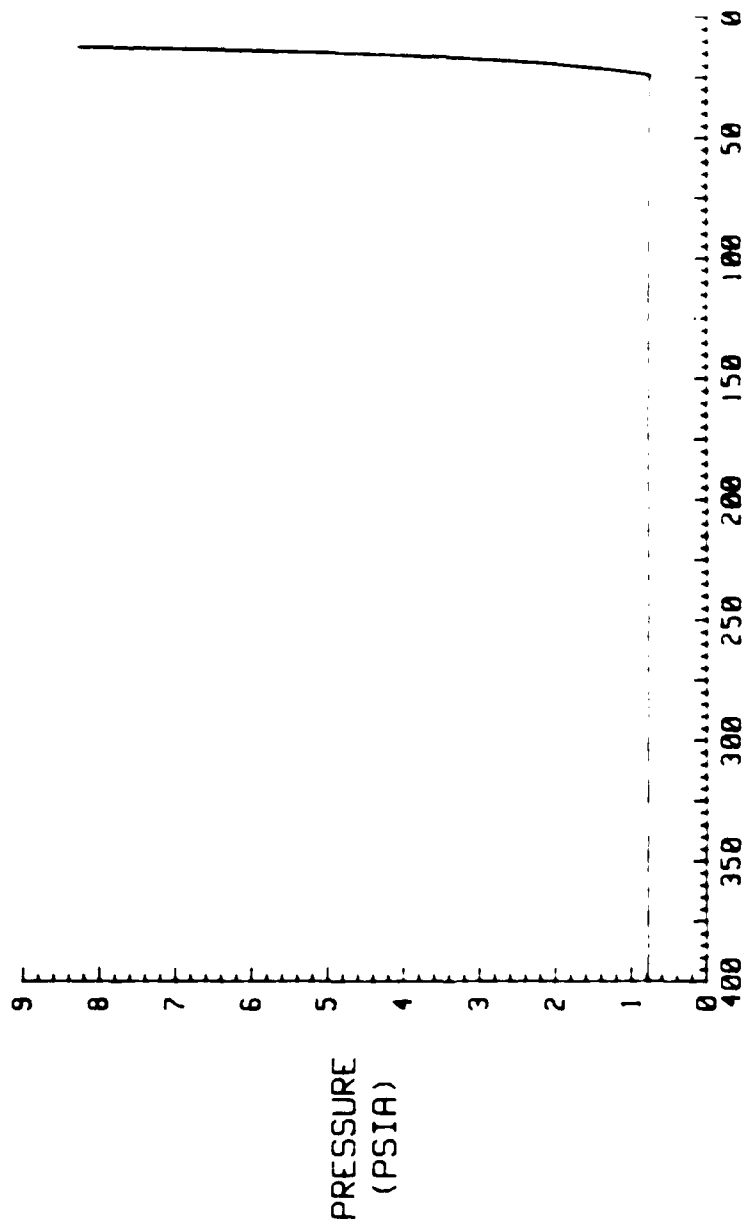


PRESSURE RATIO (PR)

FIGURE. B-7. P8 VS PR (CON2B)

PRESSURE  
(PSIA)

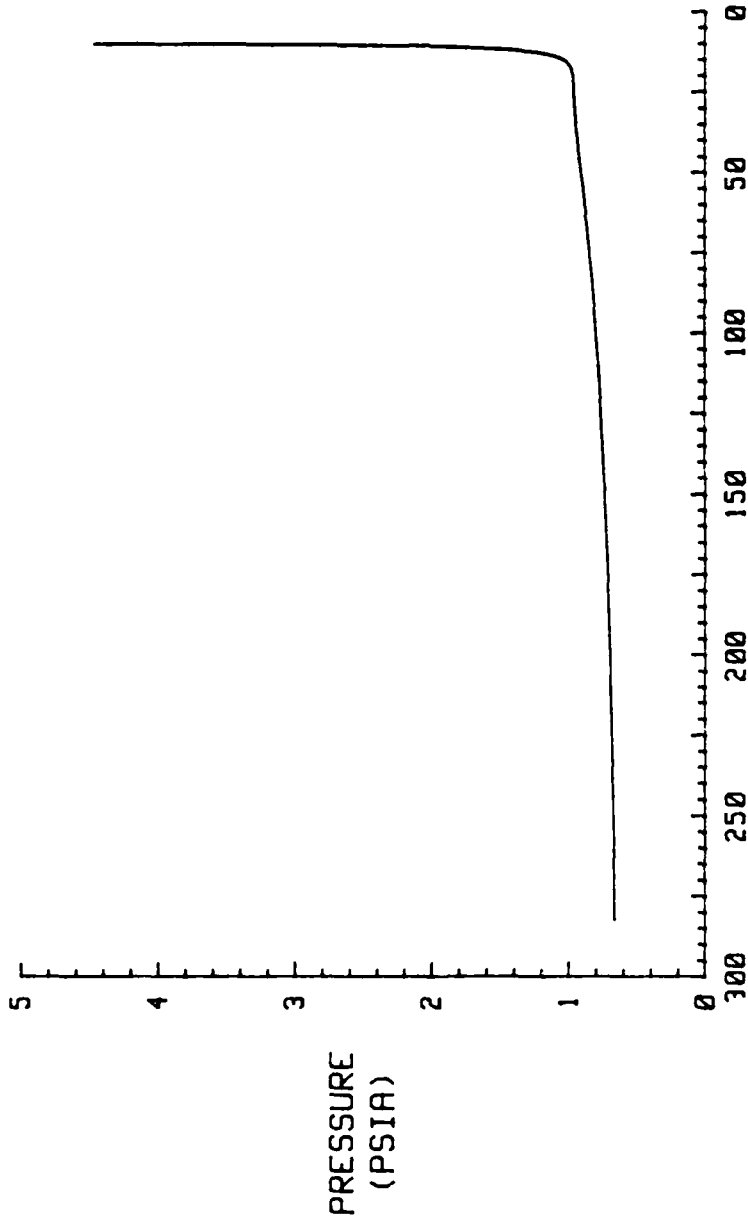
CONF IGURATION 2B



PRESSURE RATIO (PR)

FIGURE. B-8. P9 VS PR (CON2B)

CONFIGURATION 4B



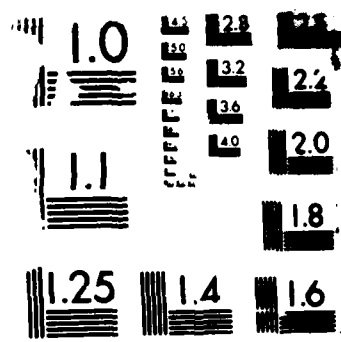
04  
PRESSURE  
(PSIA)

PRESSURE RATIO (PR)

FIGURE. B-9. P6 VS PR (CON4B)

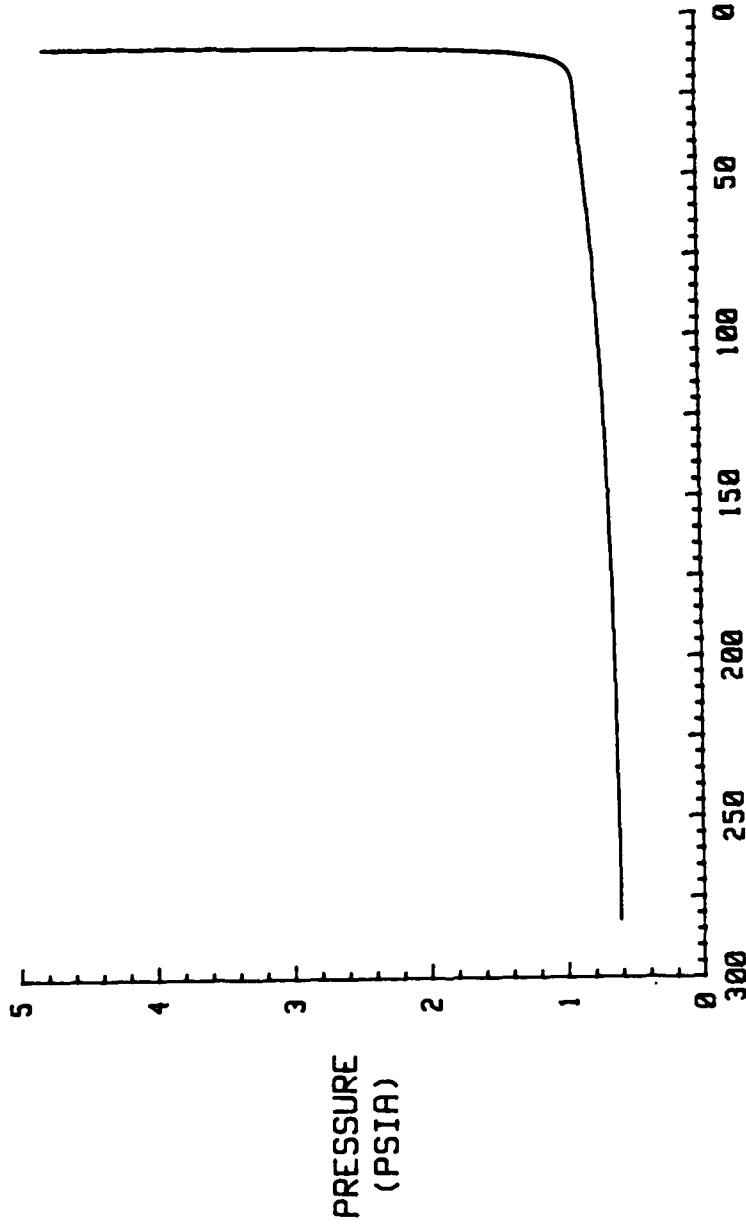
AO-A179 477 INVESTIGATION OF SHROUDED NOZZLE EXIT PRESSURE CHANGES 2/2  
(U) AIR FORCE INST OF TECH WRIGHT-PATTERSON AFB OH  
SCHOOL OF ENGINEERING D C RODGERS DEC 86  
UNCLASSIFIED AFIT/GAE/AA/86D-15 F/G 20/4 ML

■■■■■■■■■ EMI  
S-87



MI

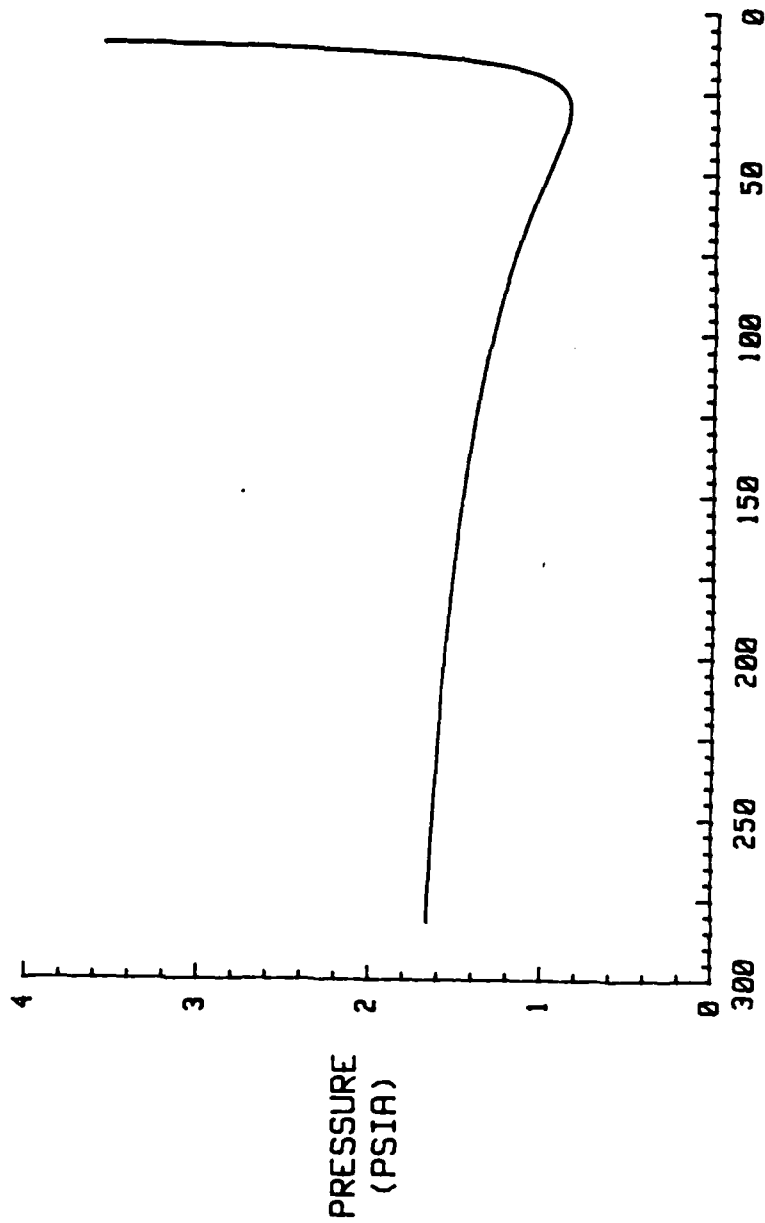
CONFIGURATION 4B



85  
PRESSURE  
(PSIA)

PRESSURE RATIO (PR)  
FIGURE. B-10. P7 VS PR (CON4B)

CONFIGURATION 4B

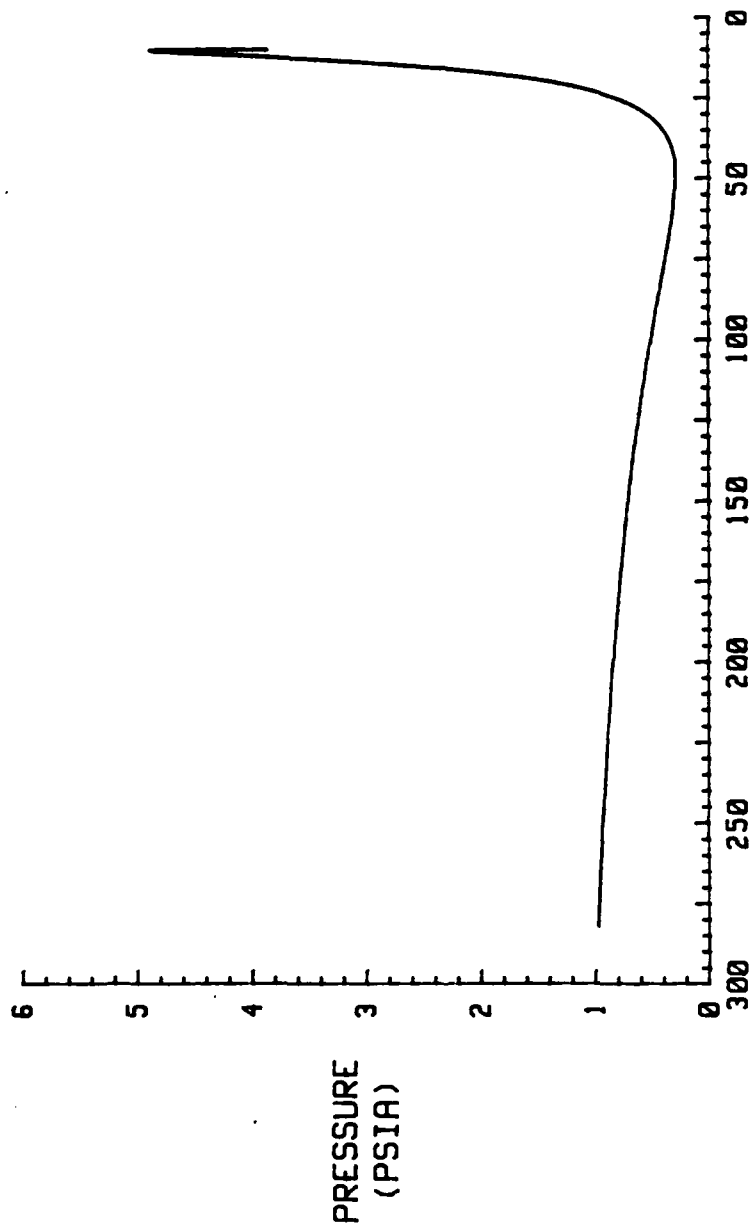


PRESSURE  
(PSIA)

86

PRESSURE RATIO (PR)  
FIGURE. B-11. P8 VS PR (CON4B)

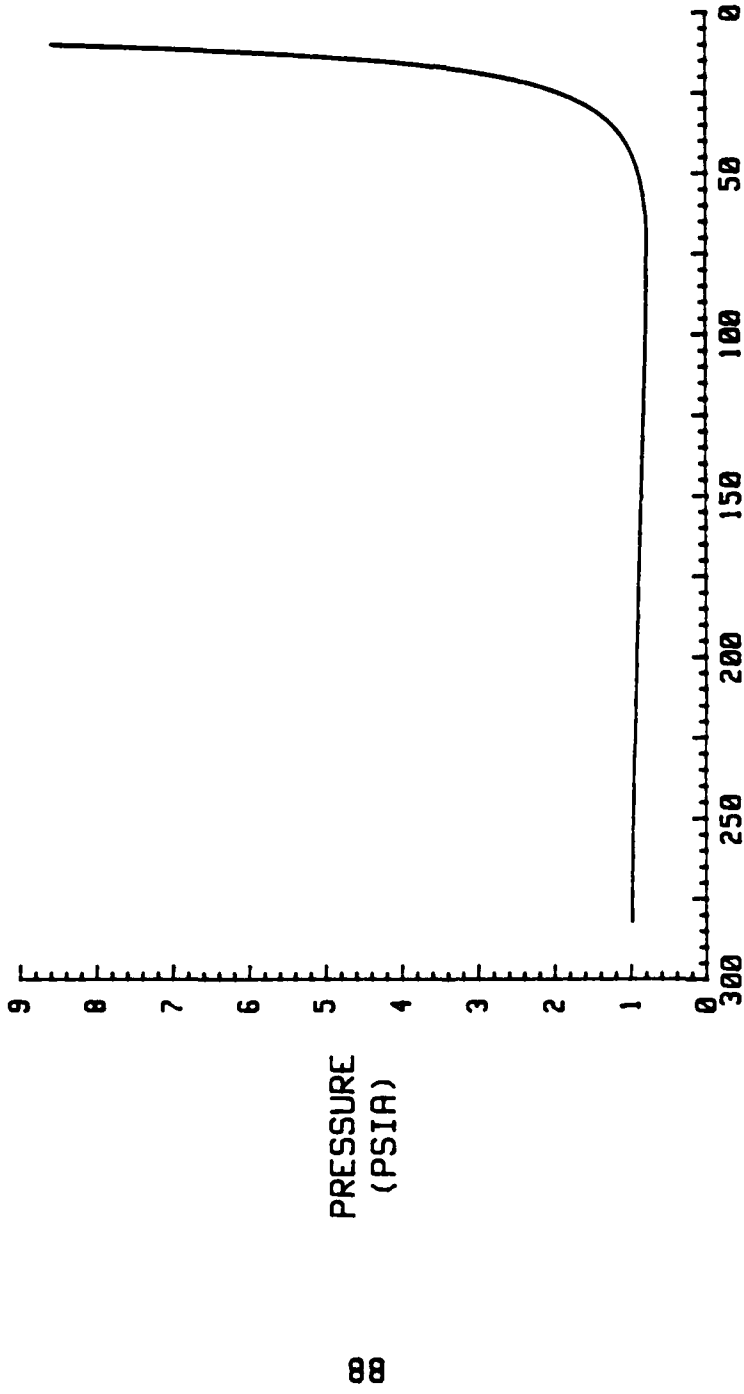
CONFIGURATION 4B



PRESSURE RATIO (PR)

FIGURE. B-12. P9 VS PR (CON4B)

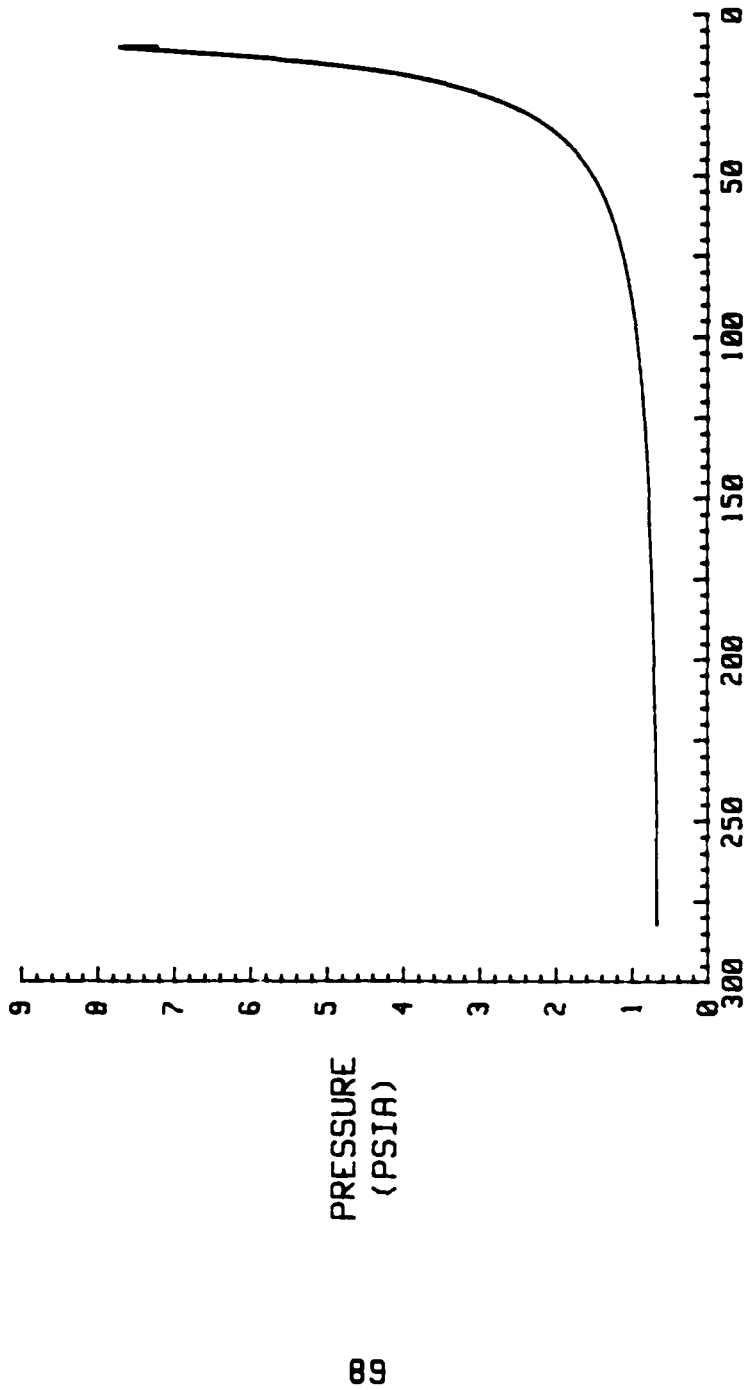
CONFIGURATION 4B



PRESSURE RATIO (PR)

FIGURE. B-13. P10 VS PR (CON4B)

CONFIGURATION 4B



PRESSURE RATIO (PR)

FIGURE. B-14. P11 VS PR (CON4B)

VITA

Captain Douglas C. Rodgers was born 11 June 1955 at Westover AFB, Massachusetts. In May 1978, he received his BS degree in Aeronautical Engineering from the United States Air Force Academy, Colorado Springs, Colorado. Upon graduation he was commissioned a 2Lt in the USAF. Following graduation from Undergraduate Navigator Training, he flew B-52G aircraft in California and served as a navigator, instructor navigator, radar navigator, instructor radar navigator, and standardization/evaluation radar navigator. Captain Rodgers entered the School of Engineering, Air Force Institute of Technology, in May 1985.

Permanent address: 3630 Carefree Place  
Colorado Springs, Colorado  
80917

A179 497

## REPORT DOCUMENTATION PAGE

Form Approved  
OMB No. 0704-0188

1a. REPORT SECURITY CLASSIFICATION UNCLASSIFIED			1b. RESTRICTIVE MARKINGS			
2a. SECURITY CLASSIFICATION AUTHORITY			3. DISTRIBUTION / AVAILABILITY OF REPORT Approved for public release; distribution unlimited.			
2b. DECLASSIFICATION / DOWNGRADING SCHEDULE						
4. PERFORMING ORGANIZATION REPORT NUMBER(S)  AFIT/GAE/AA/86D-15			5. MONITORING ORGANIZATION REPORT NUMBER(S)			
6a. NAME OF PERFORMING ORGANIZATION School of Engineering		6b. OFFICE SYMBOL (If applicable) AFIT/ENG	7a. NAME OF MONITORING ORGANIZATION			
6c. ADDRESS (City, State, and ZIP Code) Air Force Institute of Technology Wright-Patterson AFB, OH 45433			7b. ADDRESS (City, State, and ZIP Code)			
8a. NAME OF FUNDING / SPONSORING ORGANIZATION		8b. OFFICE SYMBOL (If applicable)	9. PROCUREMENT INSTRUMENT IDENTIFICATION NUMBER			
8c. ADDRESS (City, State, and ZIP Code)			10. SOURCE OF FUNDING NUMBERS			
			PROGRAM ELEMENT NO.	PROJECT NO.	TASK NO.	WORK UNIT ACCESSION NO.
11. TITLE (Include Security Classification)  See Box 19						
12. PERSONAL AUTHOR(S) Douglas C. Rodgers, Capt, USAF						
13a. TYPE OF REPORT MS Thesis		13b. TIME COVERED FROM _____ TO _____		14. DATE OF REPORT (Year, Month, Day) 1986 December	15. PAGE COUNT 90	
16. SUPPLEMENTARY NOTATION						
17. COSATI CODES			18. SUBJECT TERMS (Continue on reverse if necessary and identify by block number)  Shrouded, Clustered Nozzles, Three-Dimensional Two-Dimensional			
FIELD	GROUP	SUB-GROUP				
21	08					
19. ABSTRACT (Continue on reverse if necessary and identify by block number)  Title: Investigation of Shrouded Nozzle Exit Pressure Changes  Thesis Advisor: Dr. William C. Elrod Department of Aeronautics and Astronautics  <div style="text-align: right;">Approved for public release: IAW AFR 190-14. <i>Lyn E. Wolaver</i> April 87 LYN E. WOLAVER Dean for Research and Professional Development Air Force Institute of Technology (AFIT) Wright-Patterson AFB OH 45433</div>						
20. DISTRIBUTION / AVAILABILITY OF ABSTRACT <input type="checkbox"/> UNCLASSIFIED/UNLIMITED <input checked="" type="checkbox"/> SAME AS RPT. <input type="checkbox"/> DTIC USERS			21. ABSTRACT SECURITY CLASSIFICATION UNCLASSIFIED			
22a. NAME OF RESPONSIBLE INDIVIDUAL Dr. William C. Elrod, Professor			22b. TELEPHONE (Include Area Code) 513-255-3517		22c. OFFICE SYMBOL AFIT/ENY	

EM